Reactive oxygen species induce virus-independent MAVS-oligomerization in systemic lupus erythematosus

One sentence summary: Oxidative stress induces cysteine 79-dependent oligomerization of MAVS in lymphocytes and plasma of SLE patients

Iwona A. Buskiewicz[1]*, Theresa Montgomery[1], Elizabeth C. Yasewicz[1], Sally A. Huber[1], Michael P. Murphy[3], Richard C. Hartley[4], Ryan Kelly[5], Mary K. Crow[6], Andras Perl[5], Ralph C. Budd[2], and Andreas Koenig[1,2]*

Departments of [1]Pathology and [2]Medicine, Vermont Center for Immunology and Infectious Diseases, University of Vermont, Burlington, VT 05405; [3]MRC Mitochondrial Biology Unit, Wellcome Trust/MRC Building, Cambridge, CB2 0XY, UK; [4]WestCHEM School of Chemistry, University of Glasgow, Glasgow G12 8QQ, UK; [5]Upstate University Hospital, State University of New York, Rheumatology Clinic, Syracuse, NY 13202, [6]Hospital for Special Surgery, Weill Cornell Medical College, New York, NY 10021

*Corresponding authors: Dr. Andreas Koenig (akoenig@uvm.edu), Department of Medicine-Immunobiology and Department of Pathology; Dr. Iwona A. Buskiewicz (ibuskiew@uvm.edu), Department of Pathology, University of Vermont, 89 Beaumont Avenue, Given Building D-211, Burlington, VT 05405

ABSTRACT

Upregulation of type I Interferon (IFN-I)-induced genes is characteristic of both viral infections and Systemic lupus erythematosus (SLE). Here we show that mitochondrial antiviral signaling protein (MAVS), which normally forms a complex with retinoic acid gene I (RIG-I)-like helicases during viral infection, can be activated by oxidative stress alone, independent of RIG-I helicases. We observe that chemically generated oxidative stress induces MAVS oligomerization, which leads to mitochondrial hyperpolarization, decreased ATP production, and decreased spare respiratory capacity not observed otherwise in cells lacking MAVS. Peripheral blood lymphocytes of SLE patients, which also have increased oxidative stress, manifest spontaneous MAVS oligomerization that correlates with increased IFN-I. Consistent with this, inhibition of mitochondrial reactive oxygen species (ROS) by the mitochondria-targeted antioxidant MitoQ prevented oligomerization of MAVS and IFN-I production. Furthermore, ROS-mediated MAVS oligomerization and IFN-I production was reduced in cells expressing a MAVS-C79F variant that occurs in 30% of sub-Saharan Africans and has been linked with reduced secretion of IFN-I and milder SLE. These MAVS-C79F SLE patients also had reduced oligomerized MAVS. Collectively, our findings suggest that spontaneous MAVS oligomerization due to mitochondrial oxidative stress in SLE patients contributes to the IFN-I signature characteristic of this syndrome.

INTRODUCTION

Oxidative stress characterizes several infectious and autoimmune diseases, reflecting a disturbance in the normally tightly regulated balance between the production of various chemically reactive molecules, such as reactive oxygen species (ROS) and reactive nitrogen species (RNS), and antioxidants, including the glutathione and thioredoxin systems (*1*). During the early stages of certain RNA virus infections, retinoic acid gene I (RIG-I)-like helicases (RLHs) sense and bind to viral RNAs. RIG-I–RNA complexes associate with mitochondrial antiviral signaling protein (MAVS), which is located on the cytoplasmic face of the outer mitochondrial membrane (*2*). The interaction between RIG-I and MAVS is facilitated by mutual N-terminal caspase recruitment domains (CARD). RIG-I–MAVS complex formation then leads to CARD-dependent MAVS oligomerization and the subsequent activation of IFN-I regulatory factors (IRFs) 3 and 7 and nuclear factor-κB (NF-κB), which in turn induces the production of IFN-I and proinflammatory cytokines (*3, 4*). Recent findings suggest that the homeotypic CARD interaction of MAVS with the CARD of RIG-I can form protein aggregates and filaments on the surface of the mitochondria that can further activate MAVS proteins into functional clusters on the outer mitochondrial membrane (*5*). These high-molecular-weight MAVS complexes amplify the formation of the cytosolic signaling complex that activates IRFs and NF-κB (*5, 6*).

Virus-induced MAVS aggregates are resistant to treatment with protease and detergent but are sensitive to reducing agents such as dithiothreitol (DTT) or ² -mercaptoethanol (² -Me) early in the induction process, suggesting that disulfide bond formation contributes to MAVS oligomer formation and stability (*5*). MAVS oligomerization may thus be a redox sensitive process. Reactive oxygen species (ROS) can modulate the

expression of a variety of inflammatory processes (*7-9*), and the recent finding that increased cellular ROS amplifies RIG-I signaling and MAVS function at the mitochondria supports this notion (*5, 10*). Accordingly, the RIG-I–MAVS signaling pathway is also enhanced by nicotinamide adenine dinucleotide phosphate (NADPH) oxidase 2 (NOX2), a cytoplasmic source of ROS (*11*). Conversely, repression of mitochondrial ROS (mROS) production by cytochrome C oxidase complex subunit 5 (COX5B) inhibits MAVS aggregation and downstream signaling (*12*). Although recent work by Xu, et al. (*6*) defined the structural basis of the MAVS–CARD self-interaction, it is currently unknown as to how MAVS oligomerization might occur in response to oxidative stress in the absence of viral infection (*6*).

A recent study by one of our groups showed that peripheral blood lymphocytes (PBL), particularly T cells, from patients with systemic lupus erythematosus (SLE) show an increase in ROS with corresponding mitochondrial hyperpolarization and increased mitochondrial electron transport chain activity at complex I (*13*). In turn, enhanced mROS production leads to oxidative modifications of many cellular proteins, lipids, and DNA (*14, 15*). Moreover, the depletion of cytosolic ATP associated with mitochondrial hyperpolarization predisposes T lymphocytes to death by necrosis in SLE (*16-22*). Increased amounts of serum IFN-I in SLE patients were first reported over 20 years ago (*23*), but only recently has the role of IFN-I in the pathogenesis of SLE been fully appreciated (*24*). More than half of SLE patients display excess production of IFN-I and upregulation of a group of IFN-I–stimulated genes that are associated with active disease (*25, 26*). Several recent observations have linked SLE risk alleles to both the production of, and response to, IFN-I (*27*). Noteworthy among these is a single nucleotide

polymorphism (SNP) in the CARD domain of MAVS that changes a cysteine to phenylalanine at position 79 (C79F) (*28*). MAVS-C79F occurs in 30% of the Sub-Saharan healthy population, and its presence in African-American SLE patients was associated with substantially reduced IFN-I, absence of autoantibodies against RNA-binding proteins, and overall milder SLE (*28*). This suggests that cysteine 79 could render MAVS susceptible to ROS-mediated modification through disulfide bridge formation among CARD domains, leading to MAVS oligomerization. Thus, those individuals bearing the MAVS-C79F variant might be somewhat protected from an overwhelming IFN-I inflammatory response to viral infections. Similarly, SLE patients with MAVS-C79F might also be protected from ROS-induced IFN-I production.

Here we report that MAVS oligomerization during viral infection leads to decreased oxygen consumption, reduced mitochondrial biogenesis, and a higher mitochondrial membrane potential, resembling the mitochondrial phenotype observed in T cells of SLE patients. We further show that chemically induces oxidative stress is sufficient to induce MAVS oligomerization, leading to significant IFN-I production. Furthermore, spontaneous MAVS oligomerization is observed in PBL and plasma of several SLE patients, but rarely in age- and sex-matched healthy controls. Additionally we show that patients with oligomerized MAVS have decreased capacity for oxidative phosphorylation and increased plasma IFN-I. MAVS oligomerization can also be inhibited by the mitochondria-targeted antioxidant MitoQ. Additional analysis revealed that ROS-induced oligomerization of MAVS and consequent IFN-I production are greatly reduced in cell lines expressing the MAVS-C79F variant but not significantly during viral infection. Consistent with this, SLE patients bearing the MAVS-C79F variant had reduced MAVS

oligomerization. Together these findings suggest a mechanism by which mitochondrial dysfunction and oxidative stress can result in the IFN-I signature of SLE patients via MAVS oligomerization.

RESULTS

MAVS oligomerization decreases ATP production and mitochondrial spare respiratory capacity. ROS and redox-regulating proteins such as COX5B or NOX2 that can modify mitochondrial and cytoplasmic ROS quantity, respectively, can regulate the MAVS-mediated antiviral pathway through altering the expression of MAVS itself (*12*). However, the role of MAVS depletion or cleavage in cellular mitochondrial oxidative metabolism has not been investigated. Thus, we examined mitochondrial function and metabolism in wild-type (WT) or MAVS-deficient (MAVS-KO) mouse embryonic fibroblasts (MEFs) during infection with either Coxsackievirus B3 (CVB3), Sindbis virus (SINV), or after transfection with an RNA containing a triphosphate incorporated at the 5′ end (5′-ppp) that is a specific ligand for RIG-I. Both CVB3 and SINV are single-stranded, positive-sense RNA viruses with the ability to activate the RIG-I pathway (*29*). However, unlike SINV, CVB3 has the additional ability to cleave MAVS at Gln148 with its $3C^{pro}$ protease (*30*). During the initial 12 h following CVB3 and SINV infection, or 5'-ppp RNA transfection, we observed that both ROS and mitochondrial membrane potential ($\Delta\Psi_m$) increased (Fig. 1, A and B), in agreement with previous findings (*31, 32*). However, beyond the 12 h time point, in contrast to SINV and 5'-ppp-RNA, CVB3-induced cleavage of MAVS paralleled a marked reduction in cellular ROS and $\Delta\Psi_m$ (Fig. 1, A to C). Changes in $\Delta\Psi_m$ and ROS during viral infection or 5′-ppp–RNA stimulation also correlated positively with MAVS oligomerization (Fig. 1D).

Particularly striking was that no increase in ROS or $\Delta\Psi_m$ was observed during viral infection of MAVS-KO cells (Fig. 1, A and B). This was also true of cells expressing a truncated form of MAVS cleaved at Gln148, which lacks the CARD domain required for MAVS oligomerization (Fig. S1). Using the mitochondria-targeted, redox-sensitive di-cysteine green fluorescent protein (roGFP) as a probe (*33*), we determined that the increased matrix thiol oxidation during viral infection or stimulation with 5′-ppp–RNA originated primarily in mitochondria (Fig. 1E).

We observed elongation and further swelling of mitochondria following viral infection and 5'-ppp-RNA exposure (Fig. S1), consistent with previous observations (*34-36*). Mitochondrial morphological alterations that occur along with changes in mitochondrial membrane polarization can also lead to changes in respiration, and ATP production (*37*). To establish whether MAVS influences cellular metabolism during an innate immune response to viral infection, we measured total ATP production (Fig. 1F) and the ATP/ADP ratio (Fig. 1G) in MAVS-WT and MAVS-KO cells before and following infection with CVB3, or transfection with 5′-ppp–RNA. Interestingly, we observed that prior to infection MAVS-KO cells manifested a nearly 3-fold higher amount of cellular ATP than MAVS-WT cells (Fig. 1F). This high quantity of ATP in MAVS-KO cells correlated with a higher ATP/ADP ratio (Fig. 1G). Following CVB3 infection, the total ATP and ATP/ADP ratio increased 2-fold in MAVS-WT cells but did not increase further in MAVS-KO cells (Fig. 1, F and G). Increase in ATP production or the ATP/ADP ratio following CVB3 infection in MAVS-WT cells approached the total steady state of ATP in MAVS-KO cells (Fig. 1, F and G), and corresponded closely with the cleavage pattern of MAVS during CVB3 infection (Fig. 1C) is suggestive of a causative relationship.

Interestingly, we did not observe the same increase in ATP/ADP in cells transfected with 5′-ppp–RNA, which can continually activate RIG-I and MAVS oligomerization. In this case, following a small spike, the amount of ATP declined over time (Fig. 1F), suggesting that RIG-I and MAVS activation lowered the total quantity of ATP in the cells.

To further assess the bioenergetic profile during viral infection in the presence or absence of MAVS, we initially examined the oxygen consumption rate (OCR) as an indicator of oxidative phosphorylation using a Seahorse extracellular flux analyzer (*38*). To assess mitochondrial respiratory capacity we sequentially treated cells with oligomycin (to block ATP synthesis), the ionophore FCCP (to uncouple mitochondria and thereby maximally stimulate the electron transport chain (ETC)), and rotenone (to block ETC complex I) (Fig. 1H). We observed that CVB3-infection and 5′-ppp–RNA-treatment of MAVS-WT cells manifested significantly lower basal OCR than mock-treated cells, and a very minimal response to FCCP treatment, suggesting impaired spare respiratory capacity (SRC) (Fig. 1, I and J). Three hours post-infection, at a time when the CVB3 $3C^{pro}$ protease had produced only a small amount of cleaved MAVS (Fig. 1C), the metabolic profile of CVB3-infected cells did not differ from cells transfected with 5'-ppp-RNA (Fig. 1I). However, the same metabolic profile measured at 24 h when CVB3 $3C^{pro}$ had significantly cleaved MAVS, showed that CVB3-infected cells, but not 5′-ppp–RNA transfected cells, returned to basal capacity of OCR and SRC (Fig. 1J). Under the same conditions, MAVS-KO cells showed higher baseline OCR and SRC than MAVS-WT cells but, unlike MAVS-WT cells, this state did not significantly change with CVB3 infection or 5′-ppp–RNA treatment. (Fig. 1, K and L). The findings

from three separate OCR studies in MAVS-WT vs MAVS-KO MEFs is summarized in Figure 1, M and N. As prolonged cell culture can impact the phenotype of MEF, we tested whether metabolic differences are indeed due to the differences in genotype using primary splenocytes from MAVS-WT vs MAVS-KO mice and observed the same phenotype as in MEFs (Fig. 1, O and P). In contrast to the differences in oxygen consumption, the basal extracellular acidification rate (ECAR), a readout of lactate production by glycolysis, was very similar between MAVS-WT and MAVS-KO MEFs (Fig. S1). Collectively, these findings suggest that MAVS oligomerization inhibits mitochondrial respiration and ROS production.

Oxidative stress independent of viral infection induces MAVS oligomerization. To further evaluate the influence of oxidative stress on MAVS oligomerization in the presence or absence of viral infection, we used two gel systems. First, we adapted a Tris-Glycine-eXtended (TGX) gradient polyacrylamide gel system to detect with high resolution MAVS aggregates (*39*). Second, to better detect the total amount of MAVS oligomers, we used Tris-Glycine agarose gels, which allow improved migration of large molecular weight complexes (*5*). We assessed MAVS oligomerization during chemically induced oxidative stress using glucose oxidase (GOx), which generates H_2O_2 in the process of catalyzing the oxidation of glucose to D-glucono-´ -lactone, and compared it with SINV infection (*40*). At concentrations of 10–20 µg/mL, GOx increases cytoplasmic ROS at a quantity close to those observed during viral infection (*41*). We observed that GOx-mediated oxidative stress alone was sufficient to induce MAVS oligomerization, in a manner similar to SINV infection (Fig. 2A). Of interest, GOx-induced MAVS

oligomerization was reversible when cell media were supplemented with β-mercaptoethanol (β-Me) (Fig. 2A). This was much less apparent during SINV infection, where only a portion of the MAVS oligomers were reducible. This difference could reflect the fact that virus-induced oligomerization of MAVS involves both RIG-I-CARD/MAVS-CARD dimerization as well as ROS-induced MAVS oligomerization, whereas GOx involves only the latter process. To address the possibility that the observed MAVS oligomerization might be an artifact of cysteine dimerization induced during cell lysis and processing for electrophoresis, freshly prepared cells were homogenized in buffer containing iodoacetamide, which covalently binds to free thiol groups of cysteines to prevent further disulfide bond formation. The presence of 100 μM iodoacetamide did not result in a decrease in MAVS oligomers either following GOx treatment or SINV infection (Fig. S2A). MAVS oligomerization induced by GOx also led to the formation of the MAVS signaling complex as detected by co-precipitation of MAVS via its N-terminal His-tag. Within 3 h post ROS induction, we observed the association of TRAF2, TANK, TRADD, and RIPK1 with MAVS, suggesting that both interferon regulatory factors and the NF-κB branch of the MAVS signaling complex had occurred (Fig. 2B).

MAVS oligomerization induced by GOx correlated with increased $\Delta\Psi_m$ (Fig. 2C). In agreement with the ability of β-Me to reverse MAVS oligomerization, supplementation of media with β-Me also prevented mitochondrial hyperpolarization in cells treated with GOx, but not following SINV infection (Fig. 2C). MAVS oligomerization induced by GOx lead to increased secretion of IFN-β and IL-6, which was not observed in MAVS-deficient cells, but treated with the compound (Fig. 2, D and E).

To determine whether ROS derived specifically from mitochondrial respiration could also induce MAVS oligomerization, we used the compound MitoParaquat (MitoPQ), a mitochondria-targeted superoxide generator that contains a paraquat moiety tethered to a positively charged lipophilic triphenylphosphonium (TTP) cation that drives MitoPQ accumulation within negatively charged mitochondria (*42*). Treatment of MEFs with moderate concentrations of MitoPQ (1 to 10 nM) led to an increased MAVS oligomerization (Fig. 2F), without causing significant cell death at the doses used (Fig. 2G). Treatment of cells with MitoPQ also led to significant increase of IFN-β and IL-6 secretion that was not observed in MAVS-KO cells treated with MitoPQ (Fig. 2, H and I).

To further rule out a potential role of RIG-I-like receptors in the process of ROS-induced MAVS oligomerization, cells lacking either RIG-I or both RIG-I and MDA5 were treated with GOx, MitoPQ and specific ligands for RIG-I (5'-ppp-RNA) and MDA5 (poly(I:C)). As demonstrated by immunoblotting, GOx-induced MAVS oligomerization occurred in the absence of RIG-I or when both RIG-I and MDA5 were absent (Fig. 2J). MEFs lacking both RIG-I and MDA5, but not MAVS-deficient cells, showed elevation IFN-β (Fig. 2K) and IL-6 mRNA (Fig. S2B) following treatment with GOx and MitoPQ, which correlated with increased secretion of these cytokines (Fig. 2L and S2C). RIG-I, MDA5 or MAVS deficient cells treated with RIG-I or MDA5 ligands did not show an increase of IFN-β (Fig. 2, K and L) and IL-6 (Fig S2, B and C). To control whether RIG-I, MDA5 or MAVS deficient cells are capable to secrete pro-inflammatory cytokines, we have treated these cells with dsDNA, which leads to secretion of IFN-I and IL-6 in a RIG-I pathway independent manner (*43*). We have observed that dsDNA lead to equal IFN-β and IL-6

secretion in RIG-I, MDA5 or MAVS deficient cells, respectively (Fig. S2D). These findings support the view that ROS alone in the absence of viral infection is sufficient to induce MAVS oligomerization and downstream cytokine signaling independent of RIG-I and MDA5.

Mitochondria-targeted antioxidant MitoQ reduces MAVS oligomerization and IFN-I secretion. MitoQ ([10-(4,5-Dimethoxy-2-methyl-3,6-dioxo-1,4-cyclohexadien-1-yl)decyl](triphenyl)phosphonium methanesulfonate) is a mitochondria-targeted antioxidant comprised of ubiquinol/ubiquinone bound to TTP (*44*). In mitochondria, MitoQ is continually recycled to the active ubiquinol antioxidant by complex II in the respiratory chain (*44, 45*). Cells pretreated with MitoQ prior to oxidative stress showed reduced MAVS oligomerization, which was more pronounced in cells treated with GOx than with SINV infection (Fig. 3A). MitoQ treatment led to at least an 80% decrease in MAVS oligomers in cells treated with GOx, whereas in cells infected with SINV MitoQ resulted in about a 40% decrease in MAVS oligomerization (Fig. 3B). As a control, cells pretreated with dTPP, which has the same mitochondria-targeting motif as MitoQ but lacks its antioxidant properties, did not demonstrate reversal of MAVS oligomerization due to SINV or ROS induction (Fig. 3A). Similar to the findings with β-Me treatment, the results with MitoQ again suggest that the nature or intensity of MAVS oligomerization induced by direct oxidative stress might differ from that stimulated by viral infection in which there is the additional heterodimerization of RIG-I-CARD with MAVS-CARD. Decreased MAVS oligomerization in the presence of MitoQ correlated with decreased mitochondrial hyperpolarization (Fig. 3C) and reduced IFN-I secretion (Fig. 3D).

MAVS oligomerizes in human PBMCs under oxidative stress and spontaneously in SLE patients. We extended the findings in MEFs to human PBMCs from healthy donors and observed that GOx induced pronounced MAVS oligomerization that appeared to be progressive, as we identified distinct MAVS bands of ~750 and >1200 kDa (Fig. 4A). As observed in MEFs, MAVS oligomerization did not occur in PBMCs pretreated with MitoQ or grown in the presence of β-Me (Fig. 4A).

We have previously observed that lymphocytes from SLE patients exhibit spontaneous increased ROS, hyperpolarization of mitochondria, and increased cell death (*21*). We thus tested whether MAVS is spontaneously oligomerized in PBMCs from SLE patients compared to age- and sex-matched healthy controls. Spontaneous MAVS oligomerization was assessed by agarose gel separation and was identified in the PBMCs of 14 of 17 SLE patients, whereas weak oligomerization was observed in 4 of the 17 healthy controls (Fig. 4, B and D). MAVS oligomers were also detected in the plasma of 12 of 17 SLE patients but not in healthy controls (Fig. 4, C and D). To exclude the possibility that the observed MAVS oligomerization spontaneously occurred during cell isolation from blood samples we added iodoacetamide, which did not decrease the detection of MAVS oligomers in cells or plasma (Fig. S3). Iodoacetamide reduced the total thiol concentration of both PBMCs and plasma homogenates by 80% and 94%, respectively (Fig. S3). These data demonstrate that MAVS oligomers are not artificially formed during tissue homogenization and processing, and further indicate that MAVS oligomers are stable in plasma. SLE plasma contained higher IFN-I than healthy controls (Fig. 4E) and the amount of IFN-I closely paralleled the degree of plasma

MAVS oligomerization (Fig. 4F). Metabolic analysis of PBMCs of SLE and healthy controls identified no difference in basal respiration (Fig. 4G), but showed statistically reduced maximal respiration, spare respiratory capacity, and the rate of ATP synthesis in the SLE patients (Fig. 4, H to J). These findings are similar to changes in respiratory capacity we observed during MAVS oligomerization induced by viral infection (Fig. 1, I to N).

To further explore which subsets of cells within the PBMC population contributed to MAVS oligomerization in SLE patients, we fractionated PBMC into T cell, B cell, and monocyte pools, and analyzed each for the presence of MAVS aggregates. As shown in Figure 4K, for equivalent amounts of protein, T cells manifested the greatest amount of MAVS oligomers, followed by B cells with relatively little detected in monocytes. MAVS oligomers were not observed in the same cell subsets of healthy controls. These findings are consistent with our earlier findings showing that much of the increased ROS in SLE PBMC is in the T cell subset (*20*). Metabolic analysis of PBMC subsets showed that, in agreement with previously published work (*46*) that monocytes, unlike B and T cells, did not show strong oxidative phosphorylation (Fig. S4). Although basal, maximal and spare respiratory capacity were significantly reduced in both B cells and T cells of SLE patients, the reduction of these parameters in T cells was at least two -old greater (Fig. 4, L to N). Noteworthy, the rate of ATP synthesis was decreased only in T cells, not significantly in B cells, of SLE patients (Fig. 4N).

MAVS oligomerization is reduced in the MAVS-C79F variant associated with milder SLE activity. SLE patients bearing a MAVS-C79F SNP have milder disease,

lower production of IFN-I, and lack autoantibodies to RNA-binding proteins (*28*). In addition, cells expressing MAVS-C79F secrete a lesser amount of inflammatory mediators such as IL-8, RANTES, and IFN-^{2} (*28*). Since this SNP modifies a cysteine residue, we considered that this might alter the ability of MAVS-C79F to form oligomers under oxidative stress. We thus initially reconstituted MAVS-KO MEFs with either human MAVS-WT, the C79F variant, or a combination of the two (Fig. 5A). We observed that cells reconstituted with the MAVS-C79F variant manifested lower amounts of MAVS oligomerization following treatment with GOx. The same C79F cells following SINV infection did not show significant decrease in high molecular weight MAVS oligomers as compared to GOx treatment but presence of moderate size oligomers was detected whose size might reflect trimer or tetramer formation (Fig. 5, A and B). Interestingly, although we have observed differences in the amount of MAVS oligomerization between SINV and GOx, IFN-I secretion was affected following both treatments (Fig. 5C). Further, under oxidative stress, cells expressing MAVS-C79F exhibited less mROS and $\Delta\Psi_{m,}$ suggesting that this variant had little capacity to promote mitochondrial hyperpolarization (Fig. 5, D and E).

Based on these observations in MEFs, we examined MAVS oligomerization in 6 SLE MAVS-C79F patients, 4 SLE MAVS-WT patients, and 3 healthy controls, all from the original C79F SNP study (*28*), and whose plasma was frozen at the same time. We observed that MAVS oligomerization was significantly lower in the plasma of the MAVS-C79F patients, compared to SLE patients bearing wild-type MAVS (Fig. 5, F and G).

MAVS oligomers from SLE patients can induce prion-like MAVS aggregates. MAVS has been reported to form oligomers in a prion-like manner (*5, 6*). We therefore examined whether MAVS oligomers detected in the plasma of SLE patients have the ability to induce MAVS oligomerization in purified mitochondria from wild-type MEFs that were not exposed to oxidative stress. We first purified the plasma MAVS oligomer fraction by immunoprecipitation using an anti-MAVS antibody cross-linked to protein G magnetic beads (Fig. 6, A and B). Plasma samples were initially pre-incubated with protein G magnetic beads alone to remove nonspecifically bound proteins, followed by incubation with anti-MAVS protein G beads. Following purification and elution, we observed that MAVS oligomers purified from different patients' plasma had a fairly uniform molecular weight of ~1500 kDa (Fig. 6C). Purified MAVS-oligomers from patients or healthy age- and sex-matched healthy control plasma were incubated with freshly purified mitochondria from normal MEFs for 30 min in a respiration-promoting buffer. Unbound donor MAVS oligomers were then removed by re-purification of the mitochondria using anti-Tom22 magnetic beads, as illustrated in Figure 6A. As a positive control, we observed that GOx treatment of purified mitochondria induced MAVS oligomerization (Fig. 6C, lane 2), similar to treatment of intact cells (Fig. 2A). Significantly, we observed that MAVS oligomers isolated from SLE patient plasma induced MAVS oligomerization of isolated mitochondria (Fig. 6C, lane 3), and that this was significantly decreased in mitochondria pretreated with MitoQ (Fig. 6C, lane 4). Treatment of purified mitochondria with the plasma from a healthy control (C1) did not induce detectable high-molecular-weight MAVS oligomers (Fig. 6C, lane 5). As a

negative control, purified MAVS oligomers from SLE patient plasma did not associate with mitochondria isolated from MAVS-KO cells (Fig. 6C, lane 6).

To further distinguish induced oligomers of endogenous MAVS from pre-existing SLE-donor MAVS oligomers, we performed the same experiments with mitochondria from MAVS-KO MEFs that expressed His-tagged human MAVS-WT, MAVS-C79F, or a combination of the two. Following treatment with SLE MAVS-WT oligomers, we observed high-molecular-weight bands detected by the anti-His antibody, again demonstrating that donor SLE MAVS oligomers could induce aggregation of endogenous MAVS (Fig. 6D). Additionally, we observed reduced MAVS aggregation when mitochondria contained MAVS-C79F or a combination of MAVS-WT and MAVS-C79F (Fig. 6D, lanes 3 and 4). Taken together, these data show that the MAVS oligomers in the plasma of SLE patients have the ability to induce prion-like oligomerization of endogenous MAVS.

Dendritic cells take up prion-like MAVS aggregates. The ability of dendritic cells (DCs) to take up and propagate intact prions has been described (*47-49*). Observations in transmissible spongiform encephalopathies show that internalization of fluorescently labeled prions can be detected in DCs (*50*). However, experimental data defining the role that immune cells play in the possible uptake of exogenous MAVS prion-like aggregates and subsequent activation of inflammation has not been demonstrated. To examine whether human or murine DCs can internalize MAVS oligomers purified from plasma of SLE patients, we labeled MAVS with either Alexa Fluor 546 (Alx546) or Alexa

Fluor 488 (Alx488) (Fig. 7A). Prior to enriching and labeling MAVS oligomers from plasma, total plasma was first treated with protein G magnetic beads alone and filtered through 100-kDa cut-off membranes to remove non-specific small-molecular-weight oligomers and cytokines. We then bound MAVS oligomers from plasma with anti-MAVS-protein G magnetic beads and coupled them to Alx546 or Alx488 while the MAVS oligomers were still bound to the MAVS antibody tethered to magnetic beads. This effectively removed excess dye without passing the material through another size-exclusion resin. As a negative control, we also labeled plasma from healthy controls that was free of MAVS oligomers to exclude the labeling of other plasma proteins. TGX gel analysis confirmed that labeling did not affect the stability of MAVS oligomers in SLE plasma, nor did it induce it in healthy control plasma (Fig. 7A). As MAVS oligomerization was highest in patient samples P2-P4, we used these samples for further studies (Fig. 7A). Quantification of MAVS aggregate fluorescence accounted for more than 85–90% of the total monomer MAVS obtained by treatment with ^{2}-Me and detected by luminescence with a CARD domain-specific MAVS antibody.

We then examined whether labeled MAVS aggregates could be taken up by DC derived from human peripheral blood monocytes (hDC) or murine bone marrow derived DC (BMDC) (*51, 52*). As a control, we also tested BMDC derived from MAVS-KO mice. We initially used confocal microscopy to verify the rate of MAVS internalization and to note its intracellular location relative to mitochondria using MitoTracker. Alx546-MAVS aggregate uptake and detection in both human hDCs and BMDCs occurred within 1 h (Fig. 7, B and C). We did not observe Alx546 cytoplasmic staining in DCs treated with Alx546-labeled plasma samples from healthy controls, as freely diffusing, non-

associated MAVS yield significantly weaker fluorescence. (Fig. 7B). In contrast, exogenous MAVS oligomers required the presence of endogenous MAVS in order to associate with mitochondria, and to induce IFN-I production from host cells. The increase in intracellular MAVS-fluorescence stems from the localization and association of exogenous MAVS with mitochondria, which results in an increase of local fluorescence signal. Calculation of the colocalization correlation coefficient of Alx546-MAVS and MitoTracker-green fluorescence demonstrated an association of exogenous MAVS and mitochondria, however this was substantially reduced in MAVS-KO BMDC (Fig. 7D). Mitochondrial colocalization of internalized MAVS aggregates also closely paralleled induced amounts of IFN-I secretion in wild-type BMDC, and was not detected in MAVS-KO BMDC. In addition, IFN-I was induced using MAVS aggregates from SLE patients (P2-P4), but not using healthy control plasma (C1, C2) (Fig. 7E).

We further confirmed the association of internalized exogenous MAVS with mitochondria and endogenous MAVS by purifying mitochondria from BMDC. We observed that labeled MAVS oligomers from the plasma of the SLE patients, but not healthy control plasma, induced endogenous MAVS oligomerization (Fig. 7F, upper panel). We confirmed the presence of exogenous SLE MAVS aggregates in the mitochondrial fraction by direct detection of labeled Alx488-MAVS in the gel. In agreement with the experiments performed using isolated mitochondria, we could not observe MAVS oligomers in the mitochondrial fraction of BMDCs isolated from MAVS-KO mice (Fig. 7F, lower panel). To control whether the fluorophore treatment alone of DCs could promote spontaneous MAVS oligomerization, we treated BMDCs with free

Alx488-fluorophore, which did not lead to increased MAVS expression or oligomerization (Fig. 7G). This demonstrated that any increased MAVS oligomerization following treatment with purified MAVs oligomers detected in samples P2-P4 originated from either the association of exogenous MAVS aggregate with endogenous MAVS on mitochondria or prion-like induced oligomerization.

Finally, we observed that treatment of mitochondria isolated from BMDC with purified MAVS aggregates from SLE plasma (P1-P4), but not healthy controls (C1), resulted in increased mitochondrial colocalization of MAVS signaling complex proteins TRAF2, TANK, TRADD, and RIPK1, and the formation of active IRF3 dimers (Fig. 7H), consistent with the earlier findings for IFN-I secretion from BMDCs (Fig. 7E).

DISCUSSION

The current findings support a model in which oxidative stress alone can induce the oligomerization of MAVS, resulting in the activation of IFN-I and NF-κB pathways. The fact that spontaneous MAVS oligomerization is observed in the PBMCs of SLE patients provides an important mechanistic link between the observations of increased oxidative stress and mitochondrial dysfunction in SLE lymphocytes and the known IFN-I signature found in many SLE patients (*53*). This could suggest viral- and RNA-independent activation of MAVS and IFN-I in SLE. The findings also readily suggest that antioxidants, which can inhibit MAVS oligomerization, might be therapeutic in SLE. Such clinical trials have in fact been initiated (*54*). Finally, the inability of the MAVS-

C79F variant to oligomerize under oxidative stress potentially explains why this variant is associated with milder forms of SLE (*28*).

Mitochondria fulfill several key functions in cellular metabolic and antiviral signaling pathways, including their central role in ATP generation. Although it has been suggested that MAVS oligomerization during viral infection or increased MAVS expression can lead to mitochondrial dysfunction and cell death (*55*), its role in mitochondrial metabolism has not been previously addressed. We observed that MAVS was critical for the induction of ROS production during viral infection, as ROS was absent in MAVS-deficient cells. This suggests a possible feed-forward mechanism in which initial MAVS oligomerization by RIG-I binding to MAVS through mutual CARD domains drives ROS, which in turn results in further MAVS oligomerization. Indeed MAVS oligomerization can directly suppress the function of mitochondrial complexes I-IV, in agreement with a recently identified interaction of COX5B with MAVS (*12*). Our findings that cells bearing oligomerized MAVS not only have a reduced rate of ATP synthesis, but also decreased mitochondrial spare respiratory capacity (SRC) is consistent with this model. SRC represents the extra available mitochondrial capacity a cell has to produce energy, and is thought to be critical for long-term cellular survival and function (*56*). In agreement with this model, CVB3-mediated cleavage of MAVS, or MitoQ treatment of cells with oligomerized MAVS, restores SRC.

These findings suggest that MAVS cleavage and the resulting restoration of mitochondrial high basal and spare respiratory capacity could help CVB3 to persist by

preventing cell death through energetic exhaustion of the cell. Our data further support the above premise by showing that cells lacking MAVS have high basal OCR and SRC and therefore could be resistant to cell death. In agreement, previous studies indicate MAVS-deficient fibroblasts are resistant to Sendai virus-induced cell death (*55*).

Our data show that both cellular and mitochondrial ROS can induce IFN-I and IL-6 secretion, which is dependent upon the presence of MAVS. Interestingly, IFN-I and IL-6 secretion is 3- to 4- fold higher in cells treated with MitoPQ than GOx, suggesting that superoxide produced in mitochondria is particularly potent in activating MAVS oligomerization. Another possible explanation is that GOx-induced ROS is more diffuse, and MAVS needs ROS to be localized in higher concentrations close to mitochondria in order to form disulfide bridges. Whether MAVS oligomerization is a secondary effect of mitochondrial dysfunction in SLE, or an initial driving force of mitochondrial dysfunction, is not known and will be further investigated. It will be of interest to determine whether treatment of SLE PBMC in culture with MitoQ, which is able to inhibit GOx-mediated MAVS oligomerization, will revive mitochondrial vitality. That MAVS oligomerization can be inhibited by antioxidants suggests its therapeutic potential for SLE. Such antioxidant trials in SLE are currently underway using N-acetylcysteine (*54*).

In agreement with antioxidant data, suggesting a redox-mediated mechanism of MAVS oligomerization, our data show that MAVS-C79F is resistant to ROS-dependent oligomer formation. A potential explanation for how ROS induces MAVS oligomerization is through induction of cysteine disulfide bonding, which is being investigated. MAVS

has several cysteine residues, five of which reside within the CARD domain, including Cys79. This could explain why MAVS-C79F fails to oligomerize with ROS, or to induce IFN-I. There may be other cysteine sites that can also form disulfide bonds, and disruption of any one could also severely disrupt the ability of MAVS to aggregate in response to ROS. Additionally, we found that although the MAVS-C79F variant does not form higher-molecular-weight oligomers under oxidative stress, dimer-, tetramer-sized MAVS-C79F may still be present. Conceivably, the C79F variant may merely alter MAVS conformation such that it cannot form oligomers. In fact, the original study describing the MAVS-C79F SNP hypothesized that this variant may alter MAVS conformation resulting in a modified interaction with downstream signaling molecules such as TRAF3 (*28*). Additionally our data suggests that the C79F variant, found in 30% of healthy Sub-Saharan population, could be a natural adaptation and a protective measure against environmentally induced oxidative stress by UV exposure, without affecting antiviral MAVS function.

In our model, ROS activates MAVS in an RIG-I helicases-independent fashion. However, recent data suggest that both MAVS and RIG-I helicases play prominent roles in SLE pathogenesis because an MDA5 gain-of-function mutant is associated with a higher IFN-I signature in several autoimmune diseases (*24, 57, 58*) and MAVS activation by endogenous retroviruses promotes T cell-independent B cell responses (*59*). It is feasible that ROS-production results in the formation of an endogenous RIG-I-helicase-stimulatory RNA ligand that then acts via RIG-I or MDA5 to activate MAVS. We were able to show that MAVS oligomerization at the early stages of exposure to

oxidative stress is independent of such a scenario, as MAVS oligomerization occurred in ROS-exposed MEF that were RIG-I-deficient and MDA5 knocked-down. However, it is feasible that MAVS oligomerization could for example lead to a release of mitochondrial RNA, which is not capped at the 5'-ends, and could in a feedback loop stimulate RIG-I helicases.

Cell type distribution can be altered in the PBMCs of SLE patients (*60*), and comparing MAVS oligomerization in whole PBMCs in patients and controls can be biased if there are cell-specific differences. Our data in agreement with previous studies suggests that T cells possessed the highest amount of spontaneously oligomerized MAVS in SLE patients. Another recent study has suggested that activation of the cGAS/STING pathway in neutrophils in SLE triggers IFN-I production and NETosis, a unique cell form of cell death (*61*). Dying cells are a likely source of plasma MAVS, given that SLE patients are known to have an increased proportion of dying cells in their PBMC. However, whether MAVS oligomerization occurs spontaneously in neutrophils needs to be determined. Our data suggest that MAVS is released into the plasma of SLE patients and then can be taken up by another cells, like for example DCs, where they act in prion like fashion to further amplify MAVS signaling and produce pro-inflammatory cytokines. It will be interesting to determine, how these prions can be eliminated by the cell and what is the stoichiometry and spatial organization of exogenous and endogenous MAVS complexes.

These collective findings suggest that MAVS oligomerization leads to a mitochondrial metabolic phenotype that could resemble the phenotype found in T lymphocytes of SLE patients, which manifest spontaneous mitochondrial hyperpolarization, increased ROS production, and diminished intracellular ATP (*21*). The increased and sustained IFN-I signature of SLE patients may be only one determinant of overall disease activity, however it is possible that MAVS oligomerization may contribute to the IFN-I signature in SLE. The detection of MAVS oligomers in SLE plasma suggests that this might be a useful diagnostic test for MAVS activation, which could identify subpopulations of SLE patients with IFN-I and dysfunctional mitochondria, which could be more responsive to antioxidant therapies.

Materials and Methods

Cell culture, mice and human subjects. MAVS-deficient and matching WT MEFs, a kind gift of Z. J. Chen (*2*), were maintained in Dulbecco's modified Eagle's medium (DMEM) (Hyclone), supplemented with 10% heat-inactivated fetal calf serum (FCS) (Hyclone), 100 mM L-glutamine (Cellgro Mediatech), and 10,000 units/mL penicillin/10 mg/mL streptomycin sulfate (Life Technologies). C57BL6 or B6;129-Mavstm1Zjc/J mice (The Jackson Laboratory) were maintained at the University of Vermont under a protocol approved by the Institutional Animal Care and Use Committee. Murine BMDCs were prepared as described by Inaba et al. (*52*). In brief, cells derived from femur bone marrow were cultured at a density of 5×10^5/mL in 10-cm plates in RPMI 1640 (HyClone), supplemented with 5% heat-inactivated FCS, 100 mmol L-glutamine, 100 mmol sodium pyruvate, 10,000 units/mL penicillin/10 mg/mL streptomycin sulfate, 5×10^{-5} mol 2-mercaptoethanol (Sigma), and 10 μg/mL GM-CSF (Life Technologies). Human subjects were enrolled under a protocol approved by the University of Vermont Institutional Review Board. Samples from 17 SLE patients fulfilling the American College of Rheumatology diagnostic criteria were studied (*62*). 16 out of 17 patients were female, and the age of study participants was 47± 3. The disease activity was assessed by the SLE disease activity index (SLEDAI) scores, ranging from 0 to 10 (*63*). Upon informed consent, primary human PBMCs were obtained from heparinized whole-blood samples from SLE patients. Control PBMCs were generated from age-, sex-, and ethnicity-matched healthy subjects. PBMCs were isolated using standard Ficoll gradient centrifugation as previously described (*64*). Cells were either used immediately to prepare lysates for immunoblotting or cultured at a density of 5×10^5/mL in a 12-well

culture plate with RPMI 1640 (HyClone), supplemented with 5% heat-inactivated FCS, 100 mmol L-glutamine, 100 mmol sodium pyruvate, and 10,000 units/mL penicillin/10 mg/mL streptomycin sulfate. Enriched monocytes from PBMCs were used to prepare hDCs using negative magnetic bead selection (Miltenyi), and were subsequently cultivated for 6 d in 10 µg/mL GM-CSF and 500 U/mL IL-4. All cells were maintained in a humidified chamber at 37°C and 5% CO_2.

Virus stocks. The CVB3 H3 strain was derived from an infectious cDNA clone as previously described (*65*). SINV strain S.A.A.R.86, a kind gift from R. E. Johnston, was derived from a genomic cDNA clone (*66*). Viral titers were determined by plaque assay (*67*). Infected MEFs were prepared by inoculating cells with CVB3 or SINV in DMEM at a multiplicity of infection (MOI) of 1. Cells remained in contact with the virus for 45 minutes to allow absorption, then washed with phosphate buffered saline, resuspended in fresh medium, and incubated for the indicated time periods before assays were performed.

Reagents. Polyinosinic-polycytidylic acid (poly(I:C)) and 5′ triphosphate double-stranded RNA (5′-ppp–dsRNA), both complexed with LyoVec, were purchased from InvivoGen. Mitochondria-targeted antioxidant MitoQ and the mitochondria-targeted superoxide generator MitoPQ, were generous gifts of M. Murphy (*44*). The control reagent TPP was purchased from Sigma. Reagents were added to cells at concentrations as indicated. GOx was purchased from Sigma and added to cultured

cells at a final concentration of 0.1 U/mL. Iodoacetamide was from Thermo Fisher, and used at a final concentration of 100 µM.

Flow cytometry. ROS generation was measured using oxidized, green-fluorescent dihydrocalcein acetoxymethylester (DHC-AM) (Life Technologies) and flow cytometry. Single-cell suspensions of MEFs were prepared and ROS was assessed with 5 µM DHC-AM staining in culture medium for 30 minutes (*68*). 25 nM of cationic cell permeant dye tetramethylrhodamine ethylester (TMRE; Life Technologies) (*69*) were used to measure $\Delta\Psi_m$. Additionally, MitoSox Red and MitoTracker Deep Red (Life Technologies) were used to measure mitochondrial ROS and mitochondrial mass, respectively. Flow cytometry was carried out on an LSRII (BD Biosciences), and FlowJo software (Tree Star) was used for analysis.

Metabolism assay. Real-time analysis of OCR and ECAR was performed with an XF-24 Extracellular Flux Analyzer (Seahorse Bioscience). Metabolic profiles were measured under basal conditions in non-buffered DMEM (Sigma) containing 25 mM glucose, 2 mM L glutamine, and 1 mM sodium pyruvate, in response to 1 µM oligomycin, 0.5 µM FCCP, and 1 µM rotenone/1 µM antimycin A (*70*). Total ATP was measured with the ATP Lite Kit (Perkin Elmer), and the ATP/ADP ratio was determined using the bioluminescence ADP/ATP Ratio Assay Kit from Sigma.

Confocal microscopy imaging. WT and MAVS-deficient MEFs were transfected using Neon Transfection System with roGFP-Mito2 (Addgene plasmid #49437). Mito-roGFP is

a green fluorescent protein that targets the mitochondrial matrix and displays rapid changes in fluorescence in response to changes in ambient redox potential (*33*). After transfection, cells were seeded on poly-L-lysine-coated coverslips (Becton Dickinson) and cultivated in DMEM overnight to allow cell recovery and expression of roGFP, before infection with CVB3 or SINV. Mitochondrial localization and morphology were defined by staining cells with 100 nM Mitotracker Deep Red (Life Technologies) for 15 min prior to fixation with 2% formaldehyde. Coverslips were embedded with Aqua-Mount Slide Mounting Media (Polysciences) and analyzed with a Zeiss LSM 510 Meta confocal laser scanning microscopy system (63× N.A. = 1.4 objective). Images were processed with Volocity 3D Image Analysis Software (Perkin Elmer).

IFN-I and proinflammatory cytokine measurement. ELISA was used to measure cytokine concentration in supernatant from cultured MEFs and BMDCs, and in sera of SLE patients and healthy control subjects. For assays, samples were centrifuged and IFN-^{2} and IL-6 were measured in triplicate using murine or human ELISA kits according to the manufacturer's instructions (PBL Biosciences). The fold change in IFN-I or IL-6 cells was calculated by directly comparing mock versus virus or chemical inducer of ROS.

Quantitative real-time PCR for IFN-I and IL-6. Total RNA from MEF was isolated using the RNeasy kit (Qiagen) according to the manufacturer' instructions, and reverse transcribed using iScript Reserve Transcription Supermix (Biorad). Expression of IFN-β and IL-6 mRNA was detected with use of iQ SYBR Green Supermix (Biorad) with pre-

validated primers as described previously (*71*). Data was analyzed using the 2” ” Ct method as described previously (*72*).

Functional reconstitution of human MAVS in MAVS-deficient MEFs. To reconstitute His-tagged human WT or C79F MAVS, 3 µg vector pIRES carrying the respective sequences, were transfected into 1 × 10^6 MAVS-deficient MEFs using Neon Transfection System (Life Technologies). To select for stably transfected cells, 2.5 µg/mL puromycin (Life Technologies) was added 24 h post-transfection for up to 5 days.

MAVS and MDA5 knock-down in MEF using siRNA. Where indicated, siRNA was used to knock-down MAVS (TRC MAVS shRNA, Thermo Fisher) in MEF, or MDA5 in RIG-I-KO MEF (psiRNA-MDA5, InvivoGen). 3 µg plasmid was transfected into 1 × 10^6 WT MEFs using Neon Transfection System (Life Technologies). To select for stably transfected cells, 2.5 µg/mL puromycin (Life Technologies) or zeocin (InvivoGen), respectively, was added 24 h post-transfection for up to 5 days.

Anti-His-tag immunoprecipitation. MEF were disrupted in lysis buffer and anti-His-tag antibody (Life Technologies) was used to immunoprecipitate MAVS. Purification of precipitated MAVS was performed on a MagMAX Express Magnetic Particle Processor (Thermo Fisher), and MAVS and co-immunoprecipitated proteins were separated by gel electrophoresis and detected by immunoblotting as indicated below.

Denaturing gel electrophoresis. Cultured MEFs or human PBMCs were lysed in a sample buffer containing 2% SDS and insoluble cell fragments were removed by centrifugation. Plasma samples derived from SLE patients were collected and stored at −20°C until gel electrophoresis. BCA protein assay (Thermo Scientific) was used to determine protein concentrations in all samples were resolved with SDS-PAGE under denaturing conditions. Gels were transferred to PVDF membranes using a Trans-Blot Turbo Transfer System (BioRad).

Semidenaturing detergent agarose gel electrophoresis (SDD-AGE). SDD-AGE was performed according to a published protocol with minor modifications (*73*). In brief, mitochondria were resuspended in sample buffer (0.5 × TBE, 10% glycerol, 2% SDS, and 0.0025% bromophenol blue) and loaded onto a vertical 1.5% agarose gel. After electrophoresis in the running buffer (1 × TBE and 0.1% SDS) for 35 min with a constant voltage of 75 V at 4°C, proteins were transferred to PVDF membranes using a Trans-Blot Turbo Transfer System (BioRad) for immunoblotting.

Immunoblot analysis (Western Blotting). PVDF membranes were blocked in 5% solution of nonfat powdered milk in Tris-buffered saline. Antibodies used were specific for MAVS and Actin (Santa Cruz); RIPK1 and TRAF2 (BD Biosciences); TANK, TRADD, RIG-I, and GAPDH (Cell Signaling); MDA5 and COX4 (Abcam), Alexa 488 (Life Technologies), and IRF3 (Thermo Fisher), respectively. Immunoreactive proteins were visualized using HRP-labeled conjugates (Jackson Immuno Research) and developed using Clarity Western ECL substrate (Biorad). Chemiluminescence was detected and

recorded using a Biorad Chemidoc instrument. Densitometric measurements were performed in Image Lab image acquisition and analysis software (Biorad).

Purification of MAVS-oligomers, mitochondrial isolation, and functional assay. MAVS antibody was covalently coupled to protein G magnetic beads (Life Technologies) using the bi-functional amine-reactive cross-linker disuccinimidyl suberate (DSS; Thermo Scientific). To avoid a sample contamination with proteins or protein complexes that nonspecifically bind to protein G, plasma samples were pre-incubated with protein G magnetic beads without the cross-linked MAVS antibody. SLE patient plasma were incubated for 6 hours, after which the magnetic beads were loaded onto a column in a magnetic field and extensively washed. After the beads were eluted, MAVS-oligomers were released from MAVS-antibody by way of increasing ionic strength buffer, lower pH and gel filtration. Functionally intact mitochondria from cultured cells were isolated as described earlier (*74*). This method comprises a mechanical cell rupture, followed by a precipitation of mitochondria from cell lysates using magnetically labeled anti-TOM22 (Miltenyi Biotec) antibody. Mitochondria were inoculated with SLE patient or healthy control plasma in a respiration-promoting buffer containing 125 mM KCl, 5.0 mM KH_2PO, pH 7.25, 15 mM ±-ketoglutarate and 2.0 mM ADP (*75, 76*). The reaction mixtures were centrifuged at 10,000 × *g* for 10 min, and the precipitates then analyzed using SDD-AGE.

Functional assay of endogenous MAVS aggregation and activation in vitro.

Prior to enriching and labeling MAVS oligomers from the plasma, total plasma was treated with protein G magnetic beads alone and filtered with 100-kDa cut-off membranes to remove non-specific small-molecular-weight oligomers and cytokines. We then bound MAVS oligomers from plasma with anti-MAVS-protein G magnetic beads and coupled them to Alx546 or Alx488 while the MAVS oligomers were still bound to the MAVS antibody tethered to magnetic beads to remove excess dye without passing the material through another size-exclusion resin. Purified MAVS oligomers from SLE patient plasma were fluorescently labeled using either Alx488- or Alx546-hydrazine (Life Technologies) Labeled MAVS oligomers were cocultivated with either BMDCs derived from WT or MAVS-deficient mice, or hDCs. Both murine BMDCs and human DCs were incubated for 1, 2, or 6 h. Confocal microscopy was used to analyze Alx546 fluorescence and its location. DCs were cultured on poly-L-lysine-coated coverslips and stained with MitoTracker Green (Life Technologies) and Hoechst 33342 prior to fixation with 4% formaldehyde to define mitochondria and nuclei.

Genotyping of SLE samples. Genomic DNA was extracted using Qiagen's DNeasy Blood and Tissue Kit per manufacture instructions. Unique genomic primers flanking MAVS Cys79 were designed using Primer-Blast (FP-CCCTGGGGGCCATATTAATCC/ RP- CATCAAATCGCCTCCGAGCA) and used both to PCR amplify and sequence exon2.

Analysis of mitochondrial morphology by transmission electron microscopy. For ultrastructural analysis, cells were fixed for 1 h at 65 °C in 2% paraformaldehyde and

2.5% glutaraldehyde (Polysciences) in 100 mM sodium cacodylate buffer, pH 7.2. Samples were washed in cacodylate buffer and then post-fixed for 1 h in 1% osmium tetroxide (Polysciences). Samples were then extensively rinsed in distilled H_2O before en bloc staining for 1 h with 1% aqueous uranyl acetate (Ted Pella). After several rinses in distilled H_2O, samples were dehydrated in a graded series of ethanol and then embedded in Eponate 12 resin (Ted Pella). Sections (95 nm in thickness) were cut with an Ultracut UC7 ultramicrotome (Leica Microsystems), then stained with uranyl acetate and lead citrate, and viewed on a JEOL 1400 transmission electron microscope (JEOL USA) equipped with an AMT XR611 high resolution 11 megapixel mid-mount CCD camera (Advanced Microscopy Techniques).

ACKNOWLEDGEMENTS

We thank J. Bunn for advice on statistical analyses. We further wish to thank E. Amiel and K. Fortner for discussions and critical comments regarding this study; M. von Turkovich, N. Bouffard and N. Bishop for assistance with confocal and electron microscopy, and D. Greenman for help with sample acquisition. Funding: This work was supported in part by research grants from the NIH (5P20 GM103496 to R.C.B, I.A.B. and A.K.; 5R01 HL086549 to S.A.H. and I.A.B.; Vermont Immunobiology and Infectious Diseases Center Pilot Project Grant to A.K.) and the Lupus Research Institute to R.C.B., I.A.B. and A.K. Author contributions: I.A.B. and A.K. conceived and designed the experiments; I.A.B., T.M., E.C.Y. and A.K. performed the experiments; M.P.M and R.C.H. advised on and provided mitochondria-targeted reagents; R.C.B., R.K., M.K.C. and A.P. provided SLE patient samples, demographic information and performed SLEDAI; S.A.H. provided CVB3. I.A.B. and A.K. analyzed the data and wrote the manuscript. Competing interests: The authors declare that they have no competing interests.

FIGURES

Figure 1. MAVS oligomerization induces ROS generation and regulates cellular metabolism. (A) Wild-type (WT, closed symbols) and MAVS-deficient (KO, open symbols) MEFs were infected with CVB3 or SINV (multiplicity of infection (MOI) = 1), or transfected with 1 µg 5'-ppp–RNA, and the total quantity of ROS was measured by FACS after 24 h using the oxidation-sensitive probe DHC (5 µM). (B) In parallel, the mitochondrial transmembrane potential ($\Delta\Psi_m$) was monitored using TMRE (25 nM). FACS data are mean (+/- SEM) of triplicate samples and are representative of three separate experiments. (C) The kinetics of MAVS cleavage in CVB3-infected MEFs was determined by immunoblotting. SINV-infected and MAVS-KO MEF served as controls. Data are representative of three independent experiments. (D) MAVS oligomerization in MEFs in response to CVB3 or SINV infection, or 5'-ppp-RNA transfection, was detected at the time points indicated using non-reducing gels and immunoblotting. Results were similar in three independent experiments. (E) To define the cellular source of ROS in CVB3-infected MEFs, Mito-roGFP-expressing MAVS-WT and MAVS-KO MEFs were analyzed 6 h following infection. MitoTracker Deep Red was used at 1 µM as a counterstain to define mitochondria. Confocal microscopic images are representative of three independent experiments. (F) Total ATP content of MAVS-WT and MAVS-KO MEFs after infection with CVB3 or transfection with 5'-ppp-RNA over a 24 h period was measured using a luminescence-based assay. ATP amounts across the 24 h period in mock infected WT or MAVS-KO cells are shown as controls. (G) Similarly, the ATP/ADP ratio in the same cells was measured 24 h after infection, or transfection, respectively. ATP and ATP/ADP ratios were determined in two independent experiments. (H)

Representative scheme, adapted from Seahorse Bioscience, of OCR measurement using a Seahorse XF24 Analyzer. Measurement of OCR in response to the injection of the ATP synthase inhibitor oligomycin, uncoupler FCCP, and complex I and III inhibitors rotenone and antimycin A, allowed for the calculation of the key metabolic parameters of basal mitochondrial respiration, maximal respiration, and spare respiratory capacity. (I-N) OCR measurements of MAVS-WT (I,J, closed symbols) and MAVS-KO (K,L, open symbols) MEFs as a function of CVB3 infection or 5'-ppp-RNA transfection. Measurements were made 3 h (I,K) or 24 h (J,L) post infection, or transfection. MAVS-WT and MAVS-KO cells were measured simultaneously in the same assay plate, and data represent three experiments shown as mean ± SEM. (M,N) Measurements of basal respiration, maximal respiration, and spare respiratory capacity in MAVS-WT (closed bars) and MAVS-KO (open bars) MEFs. (O,P) OCR measurements from splenocytes of MAVS-WT (closed symbols) and MAVS-KO (open symbols) mice. Statistical analysis performed were two-way ANOVA. Statistical analyses performed were one-way ANOVA, followed by Sidak's Multiple Comparison Test to examine pair-wise differences, two-way ANOVA, or Repeated Measures ANOVA, followed by Tukey's Multiple Comparisons Test to examine specific comparisons, as appropriate. (*$p < 0.05$, **$p<0.005$, ***$p<0.0005$, ****$p<0.00005$).

Figure 2. Virus-independent, oxidative stress induces MAVS oligomerization and IFN-I secretion. (A) MAVS oligomerization in MAVS-WT or MAVS-KO MEFs after glucose oxidase (GOx) treatment (1 U/ml) or SINV infection for 6 h was detected using semi-denaturing agarose gel electrophoresis. Data are representative of three

experiments. (B) Immunoprecipitation of MAVS was used to detect its association with TRAF2, TANK, TRADD, and RIPK1 following GOx treatment. (C) $\Delta\Psi_m$ using TMRE in response to GOx treatment or SINV infection was measured in MAVS-WT (black bars) and MAVS-KO (white bars) MEFs. The ionophore FCCP (10 nM) served as a control in WT and MAVS-deficient cells (bars overlap). Data are representative of at least three experiments. (D) IFN-I and (E) IL-6 cytokine secretion in response to GOx treatment was determined by ELISA in supernatants of MAVS-WT (black bars) and MAVS-KO (white bars) MEFs. Data are presented as fold-changes rather than absolute concentrations to enable comparability. The fold change was calculated by comparison of mock and treated cells. At least three independent experiments are included in each graph. (F) The formation of MAVS-oligomerization in response to 10 nM of the mitochondrial ROS-inducer MitoPQ was determined by immunoblotting. (G) Cell death induction by increasing concentrations of MitoPQ was determined by FACS using live-dead stain. (H) IFN-I (I) and IL-6 cytokine secretion by MAVS-WT (black bars) and MAVS-KO (white bars) MEFs induced by MitoPQ was measured by ELISA. Data are shown as mean ± SEM, and are representative of three experiments. (J) MAVS oligomerization in RIG-I-KO or RIG-I-KO/MDA5-knockdown (KD) MEFs was determined in the absence or presence of GOx. (K) Transcriptional activity and secretion of IFN-^{2} in WT (1), RIG-I-KO (2), RIG-I-KO/MDA5-KD (3) and MAVS-KO (4) MEFs in response to GOx, MitoPQ, poly(I:C) and 5'-ppp-RNA was measured by qPCR, and (L) IFN-^{2} secretion was determined using ELISA. Statistical analyses performed were one-way ANOVA, followed by Sidak's Multiple Comparison Test to examine pair-wise

differences, or Repeated Measures ANOVA, and followed by Tukey's Multiple Comparisons Test to examine specific comparisons. (*p < 0.05, **p < 0.005)

Figure 3. The mitochondria-targeted antioxidant MitoQ prevents MAVS-oligomerization. (A) MAVS-WT MEFs were pre-treated with 100 µM MitoQ before treatment with GOx or SINV infection, and semi-denaturing gel electrophoresis was used to detect MAVS monomers and oligomers. dTTP (100 µM) which lacks the anti-oxidant quinol residue served as a negative control. (B) The ratio of MAVS oligomers to monomers after GOx treatment or SINV infection, with or without MitoQ pre-treatment, was determined by densitometric measurement of immunoblots. (C) $\Delta\Psi_m$ in MEF after GOx+/-MitoQ and SINV+/-MitoQ treatment was measured by FACS using TMRE. (D) IFN-I secretion of MEF with or without MitoQ and GOx treatment or SINV infection was measured in cell culture supernatants using ELISA. Data shown are representative of three experiments, and bar graphs are mean ± SEM. Statistical analyses performed were two-way ANOVA (B, D), followed by Tukey's Multiple Comparisons Test to examine specific comparisons or one-way ANOVA (C), followed by Sidak's Multiple Comparison Test to examine pair-wise differences. (*p < 0.05, **p < 0.005).

Figure 4. Virus-independent oxidative stress induces MAVS-oligomerization in human PBMC, and SLE patients manifest spontaneous MAVS oligomerization. (A) Freshly isolated human PBMCs were treated with GOx for the times indicated, and semi-denaturing agarose gel electrophoresis was used to detect MAVS oligomerization. Cells (MitoQ) or cell lysates (^{2}-Me) were pretreated as indicated. Findings are

representative of three experiments. (B) Whole cell lysates and (C) plasma of SLE patients (n=8, P1 – P8) were detected by semi-denaturing agarose gel electrophoresis. Healthy, sex-, age-, and ethnicity-matched subjects served as controls (n=8, C1 – C8). (D) MAVS oligomerization in whole cell lysates (left panel) and plasma (right panel) of SLE patients (black circles) and healthy control subjects (white circles) was quantified by densitometric measurement of immunoblots. In WCL a ratio of MAVS monomer and oligomer was measured and in plasma MAVS oligomers were normalized to albumin. Each point represents MAVS oligomerization of one individual, which was determined in at least three independent experiments. (E) IFN-I secretion was measured by ELISA and compared to a commercially available standard plasma from healthy individual. (F) Comparison of plasma IFN-I and degree of MAVS oligomerization in SLE patients. (G-J) OCR determinations of basal respiration (G), maximal respiration (H), spare respiratory capacity (I), and ATP synthesis (J) from SLE patients (P) and healthy controls (C). (K) MAVS oligomer measurements in unfractionated whole PBMC (W), or B cell (B), T cell (T), and monocyte (M) fractions. Findings are representative of three patients and controls examined. (L-N) OCR measurements from whole PBMC (L), B cells (M), or T cells (N) of SLE patient (black bars) or healthy control (white bars). Findings are representative of three patients and three controls. Statistical analyses performed were Independent t-tests (D, E, G-J), two-way ANOVA (L-N) and Pearson's Correlation Coefficient (F). (*$p<0.05$, **$p<0.005$, ***$p<0.0005$, ****$p<0.00005$).

Figure 5. SLE MAVS-C79F SNP reduces MAVS oligomerization. (A) MAVS-WT MEFs, or MAVS-KO MEFs expressing either human MAVS-WT or the MAVS-C79F

SNP or combination of both, were infected with SINV, or exposed to GOx. MAVS aggregation was determined using 5% semi-denaturing TGX gels in sample buffer in presence or absence of 0.1% of ^{2}-Me, allowing detection of oligomers and intermediate lower molecular weight MAVS oligomers following immunoblotting. Data represent one of at least three experiments. (B-E) Quantitation of MAVS oligomers (B), IFN-I production (C), ROS (D), and mitochondrial membrane potential (E) from the same samples as in (A). (F,G) Semi-denaturating, 1.5% agarose gel analysis (F) and densitometry (G) of MAVS oligomers from plasma of healthy controls, SLE MAVS-C79F and SLE MAVS-WT patients that were taken and frozen at the same time; the total of high weight oligomers (above 1000kDa) were analyzed in 4 independent experiments and normalized to the amount of detectable albumin in plasma. Statistical analyses performed were two-way ANOVA (C-E), including interaction terms, followed by Tukey's Multiple Comparisons Test to examine specific comparisons or one-way ANOVA (G), followed by Sidak's Multiple Comparison Test to examine pair-wise differences. (*$p<0.05$, **$p<0.005$).

Figure 6. MAVS oligomers from SLE patients manifest prion-like activity. (A) Experimental design for the purification of MAVS oligomers from the plasma of SLE patients, and for the de novo reconstitution of SLE-MAVS oligomers with purified mitochondria from MAVS-WT MEFs, MAVS-KO MEFS, and MAVS-KO MEFs reconstituted with WT and/or C79F MAVS. MAVS antibody was covalently linked by Disuccinimidyl suberate (DSS) to protein G magnetic beads to precipitate MAVS oligomers. Similarly, mitochondria from MAVS-WT, MAVS-KO, and MAVS-C79F MEFs

were isolated with Tom22 antibody-conjugated magnetic beads. (B) Quality and purity of MAVS oligomers precipitated from SLE patient plasma (samples P1–P4) were assessed using gel electrophoresis. Plasma from a healthy individual (C1) served as a control. (C) Mitochondria from MAVS-WT and MAVS-KO MEFs were untreated or treated with GOx or MitoQ, and exposed to patient-derived MAVS oligomers. Mitochondrial lysates were then separated during gel electrophoresis and subsequent immunoblots were probed for the presence of MAVS oligomers. (D) Similarly, purified mitochondria harboring the MAVS-C79F variant or a mix of MAVS-WT and MAVS-C79F were also exposed to purified MAVS from an SLE patient (P2).

Figure 7. SLE-derived MAVS oligomers are internalized by DCs and induce mitochondrial MAVS aggregation. (A) SLE patient plasma-derived MAVS oligomers were labeled with Alx546 or Alx488 fluorophores. Gel electrophoresis confirmed labeling efficiency by direct excitation of the in-gel fluorescence of control (C1–C4) and patient (P1–P4) samples (upper panels). (B) Murine BMDCs or human monocyte-derive DCs (hDC) were cultivated with either SLE patient-derived fluorescent MAVS oligomers (P3) or plasma from a healthy control subject (C1). Shown are confocal microscopic images analyzing the localization of internalized Alx546-labeled MAVS oligomers. MitoTracker green (50 nM) and Hoechst 33342 (10 µg/ml) were used to define mitochondria and nuclei, respectively. (C) MAVS internalization kinetics was calculated by measuring increase in intracellular Alx546 fluorescence intensity over time as a ratio (P3/C1) following exposure to either SLE patient (P3) or healthy control (C1) labeled MAVS. Data are shown as mean ± SEM. (D) Correlation coefficients for mitochondria

(MitoTracker green) and Alx546-labeled MAVS oligomers were calculated to determine the co-localization of mitochondria and MAVS oligomers. For data collection, 200 individual cells were examined. (E) IFN-I secretion in response to MAVS internalization from SLE patients (P2-P4) or healthy controls (C1, C2) using BMDC from WT or MAVS-KO mice was measured by ELISA. (F) MAVS oligomerization in the mitochondrial fraction of BMDCs, which were exposed to SLE patient-derived and fluorescently labeled MAVS (top panel). Total mitochondrial MAVS was detected following treatment with reducing agent β-Me. The interaction of the patient-derived MAVS-oligomers with mitochondria was confirmed by the detection of the fluorophore using an anti-Alx488 antibody or direct in-gel fluorescence (middle panel). Mitochondrial BMDC fractions from mice lacking MAVS served as controls (lower panels). (G) To verify that neither MAVS expression nor MAVS oligomerization could be induced by the fluorophore alone, BMDCs were treated with increasing concentrations of free Alx488 dye and the mitochondrial fraction was probed for the amount of MAVS at mitochondria, and Alx488 was detected by anti-Alx488 antibody. (H) The mitochondrial fraction of BMDCs exposed to SLE patient (P2–P4) and control (C1) plasma-derived MAVS oligomers was immunoblotted to determine recruitment of signaling molecules downstream of MAVS activation. Shown immunoblots are representative of three experiments. Statistical analyses performed were two-way ANOVA (C-E), followed by Tukey's Multiple Comparisons Test to examine specific comparisons. (**$p < 0.005$).

Table 1. Genotype and activity of SLE patients

Patient	1	2	3	4	5	6	7	8	9	10	11	12	13	14	15	16	17
C79F	-	-	-	-	-	-	-	nd	nd	-	-	nd	nd	-	-	-	-
Q93E	+	-	-	-	+	+	-	nd	nd	-	-	nd	nd	-	-	+	-
MAVS	+	+	+++	+	++++	+	+++	++	+++	++	+++	++	-	+	-	-	++
IFN-I	+	+	++++	+	++++	+	+++	+++	++++	++++	+++	++++	+	+	-	++	++
SLEDAI	4	6	10	0	4	0	4	7	12	9	6	8	6	4	4	0	0

MAVS oligomerization and IFN-I change were normalized among all 17 patients, where the highest patient value was defined as 1. MAVS oligomerization and IFN-I per patient were scored with +, ++, +++, ++++, when the absolute mean value after normalization was falling between 0 and 0.25, 0.25 and 0.5, 0.5 and 0.75 or 0.75 and 1.00 respectively. (nd – not determined)

REFERENCES

1. W. Droge, Free radicals in the physiological control of cell function. *Physiol Rev* **82**, 47-95 (2002).

2. R. B. Seth, L. Sun, C. K. Ea, Z. J. Chen, Identification and characterization of MAVS, a mitochondrial antiviral signaling protein that activates NF-kappaB and IRF 3. *Cell* **122**, 669-682 (2005).

3. H. Kumar *et al.*, Essential role of IPS-1 in innate immune responses against RNA viruses. *The Journal of experimental medicine* **203**, 1795-1803 (2006).

4. T. Kawai *et al.*, IPS-1, an adaptor triggering RIG-I- and Mda5-mediated type I interferon induction. *Nature immunology* **6**, 981-988 (2005).

5. F. Hou *et al.*, MAVS forms functional prion-like aggregates to activate and propagate antiviral innate immune response. *Cell* **146**, 448-461 (2011).

6. H. Xu *et al.*, Structural basis for the prion-like MAVS filaments in antiviral innate immunity. *eLife* **3**, e01489 (2014).

7. M. Sundaresan, Z. X. Yu, V. J. Ferrans, K. Irani, T. Finkel, Requirement for generation of H2O2 for platelet-derived growth factor signal transduction. *Science* **270**, 296-299 (1995).

8. R. Gonzalez-Dosal *et al.*, HSV infection induces production of ROS, which potentiate signaling from pattern recognition receptors: role for S-glutathionylation of TRAF3 and 6. *PLoS pathogens* **7**, e1002250 (2011).

9. K. J. Tsai *et al.*, Impaired production of nitric oxide, superoxide, and hydrogen peroxide in glucose 6-phosphate-dehydrogenase-deficient granulocytes. *FEBS letters* **436**, 411-414 (1998).

10. M. C. Tal *et al.*, Absence of autophagy results in reactive oxygen species-dependent amplification of RLR signaling. *Proceedings of the National Academy of Sciences of the United States of America* **106**, 2770-2775 (2009).

11. A. Soucy-Faulkner *et al.*, Requirement of NOX2 and reactive oxygen species for efficient RIG-I-mediated antiviral response through regulation of MAVS expression. *PLoS pathogens* **6**, e1000930 (2010).

12. Y. Zhao *et al.*, COX5B regulates MAVS-mediated antiviral signaling through interaction with ATG5 and repressing ROS production. *PLoS pathogens* **8**, e1003086 (2012).

13. E. Doherty, Z. Oaks, A. Perl, Increased mitochondrial electron transport chain activity at complex I is regulated by N-acetylcysteine in lymphocytes of patients

with systemic lupus erythematosus. *Antioxidants & redox signaling* **21**, 56-65 (2014).

14. H. Ahsan, A. Ali, R. Ali, Oxygen free radicals and systemic autoimmunity. *Clinical and experimental immunology* **131**, 398-404 (2003).

15. D. Shah, N. Mahajan, S. Sah, S. K. Nath, B. Paudyal, Oxidative stress and its biomarkers in systemic lupus erythematosus. *J Biomed Sci* **21**, 23 (2014).

16. A. Perl, P. Gergely, Jr., K. Banki, Mitochondrial dysfunction in T cells of patients with systemic lupus erythematosus. *Int Rev Immunol* **23**, 293-313 (2004).

17. A. Perl, P. Gergely, Jr., G. Nagy, A. Koncz, K. Banki, Mitochondrial hyperpolarization: a checkpoint of T-cell life, death and autoimmunity. *Trends in immunology* **25**, 360-367 (2004).

18. A. Perl *et al.*, Apoptosis and mitochondrial dysfunction in lymphocytes of patients with systemic lupus erythematosus. *Methods Mol Med* **102**, 87-114 (2004).

19. K. Alam, Moinuddin, S. Jabeen, Immunogenicity of mitochondrial DNA modified by hydroxyl radical. *Cellular immunology* **247**, 12-17 (2007).

20. P. Gergely, Jr. *et al.*, Mitochondrial hyperpolarization and ATP depletion in patients with systemic lupus erythematosus. *Arthritis and rheumatism* **46**, 175-190 (2002).

21. P. Gergely, Jr. *et al.*, Persistent mitochondrial hyperpolarization, increased reactive oxygen intermediate production, and cytoplasmic alkalinization characterize altered IL-10 signaling in patients with systemic lupus erythematosus. *Journal of immunology* **169**, 1092-1101 (2002).

22. Z. W. Lai *et al.*, Mechanistic target of rapamycin activation triggers IL-4 production and necrotic death of double-negative T cells in patients with systemic lupus erythematosus. *Journal of immunology* **191**, 2236-2246 (2013).

23. S. R. Ytterberg, T. J. Schnitzer, Serum interferon levels in patients with systemic lupus erythematosus. *Arthritis and rheumatism* **25**, 401-406 (1982).

24. M. K. Crow, Type I Interferon in the Pathogenesis of Lupus. *Journal of immunology* **192**, 5459-5468 (2014).

25. E. C. Baechler *et al.*, Interferon-inducible gene expression signature in peripheral blood cells of patients with severe lupus. *Proceedings of the National Academy of Sciences of the United States of America* **100**, 2610-2615 (2003).

26. H. Zhuang *et al.*, Association of anti-nucleoprotein autoantibodies with upregulation of Type I interferon-inducible gene transcripts and dendritic cell

maturation in systemic lupus erythematosus. *Clinical immunology* **117**, 238-250 (2005).

27. L. Ronnblom, G. V. Alm, M. L. Eloranta, The type I interferon system in the development of lupus. *Semin Immunol* **23**, 113-121 (2011).

28. J. Pothlichet *et al.*, A loss-of-function variant of the antiviral molecule MAVS is associated with a subset of systemic lupus patients. *EMBO molecular medicine* **3**, 142-152 (2011).

29. V. Hornung *et al.*, 5'-Triphosphate RNA is the ligand for RIG-I. *Science* **314**, 994-997 (2006).

30. A. Mukherjee *et al.*, The coxsackievirus B 3C protease cleaves MAVS and TRIF to attenuate host type I interferon and apoptotic signaling. *PLoS pathogens* **7**, e1001311 (2011).

31. X. Si *et al.*, Pyrrolidine dithiocarbamate reduces coxsackievirus B3 replication through inhibition of the ubiquitin-proteasome pathway. *Journal of virology* **79**, 8014-8023 (2005).

32. L. Silva da Costa, A. P. Pereira da Silva, A. T. Da Poian, T. El-Bacha, Mitochondrial bioenergetic alterations in mouse neuroblastoma cells infected with Sindbis virus: implications to viral replication and neuronal death. *PloS one* **7**, e33871 (2012).

33. G. T. Hanson *et al.*, Investigating mitochondrial redox potential with redox-sensitive green fluorescent protein indicators. *The Journal of biological chemistry* **279**, 13044-13053 (2004).

34. K. Yasukawa *et al.*, Mitofusin 2 inhibits mitochondrial antiviral signaling. *Science signaling* **2**, ra47 (2009).

35. K. Onoguchi *et al.*, Virus-infection or 5'ppp-RNA activates antiviral signal through redistribution of IPS-1 mediated by MFN1. *PLoS pathogens* **6**, e1001012 (2010).

36. C. Castanier, D. Garcin, A. Vazquez, D. Arnoult, Mitochondrial dynamics regulate the RIG-I-like receptor antiviral pathway. *EMBO reports* **11**, 133-138 (2010).

37. P. A. Parone *et al.*, Preventing mitochondrial fission impairs mitochondrial function and leads to loss of mitochondrial DNA. *PloS one* **3**, e3257 (2008).

38. M. Wu *et al.*, Multiparameter metabolic analysis reveals a close link between attenuated mitochondrial bioenergetic function and enhanced glycolysis dependency in human tumor cells. *American journal of physiology. Cell physiology* **292**, C125-136 (2007).

39. K. M. Monteiro *et al.*, Echinococcus granulosus antigen B structure: subunit composition and oligomeric states. *PLoS Negl Trop Dis* **6**, e1551 (2012).

40. Q. H. Gibson, B. E. Swoboda, V. Massey, Kinetics and Mechanism of Action of Glucose Oxidase. *The Journal of biological chemistry* **239**, 3927-3934 (1964).

41. W. S. Chong *et al.*, Midazolam protects B35 neuroblastoma cells through Akt-phosphorylation in reactive oxygen species derived cellular injury. *Korean J Anesthesiol* **62**, 166-171 (2012).

42. E. L. Robb *et al.*, Selective superoxide generation within mitochondria by the targeted redox cycler MitoParaquat. *Free radical biology & medicine* **89**, 883-894 (2015).

43. L. Sun, J. Wu, F. Du, X. Chen, Z. J. Chen, Cyclic GMP-AMP synthase is a cytosolic DNA sensor that activates the type I interferon pathway. *Science* **339**, 786-791 (2013).

44. G. F. Kelso *et al.*, Selective targeting of a redox-active ubiquinone to mitochondria within cells: antioxidant and antiapoptotic properties. *The Journal of biological chemistry* **276**, 4588-4596 (2001).

45. A. M. James, H. M. Cocheme, R. A. Smith, M. P. Murphy, Interactions of mitochondria-targeted and untargeted ubiquinones with the mitochondrial respiratory chain and reactive oxygen species. Implications for the use of exogenous ubiquinones as therapies and experimental tools. *The Journal of biological chemistry* **280**, 21295-21312 (2005).

46. P. A. Kramer, S. Ravi, B. Chacko, M. S. Johnson, V. M. Darley-Usmar, A review of the mitochondrial and glycolytic metabolism in human platelets and leukocytes: implications for their use as bioenergetic biomarkers. *Redox Biol* **2**, 206-210 (2014).

47. R. Castro-Seoane *et al.*, Plasmacytoid dendritic cells sequester high prion titres at early stages of prion infection. *PLoS pathogens* **8**, e1002538 (2012).

48. C. Langevin, K. Gousset, M. Costanzo, O. Richard-Le Goff, C. Zurzolo, Characterization of the role of dendritic cells in prion transfer to primary neurons. *The Biochemical journal* **431**, 189-198 (2010).

49. N. A. Mabbott, F. Mackay, F. Minns, M. E. Bruce, Temporary inactivation of follicular dendritic cells delays neuroinvasion of scrapie. *Nature medicine* **6**, 719-720 (2000).

50. A. C. Magalhaes *et al.*, Uptake and neuritic transport of scrapie prion protein coincident with infection of neuronal cells. *The Journal of neuroscience : the official journal of the Society for Neuroscience* **25**, 5207-5216 (2005).

51. M. Dauer *et al.*, Mature dendritic cells derived from human monocytes within 48 hours: a novel strategy for dendritic cell differentiation from blood precursors. *Journal of immunology* **170**, 4069-4076 (2003).

52. K. Inaba *et al.*, Generation of large numbers of dendritic cells from mouse bone marrow cultures supplemented with granulocyte/macrophage colony-stimulating factor. *The Journal of experimental medicine* **176**, 1693-1702 (1992).

53. A. Perl, Oxidative stress in the pathology and treatment of systemic lupus erythematosus. *Nature reviews. Rheumatology* **9**, 674-686 (2013).

54. Z. W. Lai *et al.*, N-acetylcysteine reduces disease activity by blocking mammalian target of rapamycin in T cells from systemic lupus erythematosus patients: a randomized, double-blind, placebo-controlled trial. *Arthritis and rheumatism* **64**, 2937-2946 (2012).

55. Y. Lei *et al.*, MAVS-mediated apoptosis and its inhibition by viral proteins. *PloS one* **4**, e5466 (2009).

56. D. G. Nicholls, Spare respiratory capacity, oxidative stress and excitotoxicity. *Biochemical Society transactions* **37**, 1385-1388 (2009).

57. T. Robinson *et al.*, Autoimmune disease risk variant of IFIH1 is associated with increased sensitivity to IFN-alpha and serologic autoimmunity in lupus patients. *Journal of immunology* **187**, 1298-1303 (2011).

58. G. I. Rice *et al.*, Gain-of-function mutations in IFIH1 cause a spectrum of human disease phenotypes associated with upregulated type I interferon signaling. *Nature genetics* **46**, 503-509 (2014).

59. M. Zeng *et al.*, MAVS, cGAS, and endogenous retroviruses in T-independent B cell responses. *Science* **346**, 1486-1492 (2014).

60. A. M. Becker *et al.*, SLE peripheral blood B cell, T cell and myeloid cell transcriptomes display unique profiles and each subset contributes to the interferon signature. *PloS one* **8**, e67003 (2013).

61. C. Lood *et al.*, Neutrophil extracellular traps enriched in oxidized mitochondrial DNA are interferogenic and contribute to lupus-like disease. *Nature medicine* **22**, 146-153 (2016).

62. E. M. Tan *et al.*, The 1982 revised criteria for the classification of systemic lupus erythematosus. *Arthritis and rheumatism* **25**, 1271-1277 (1982).

63. C. Bombardier, D. D. Gladman, M. B. Urowitz, D. Caron, C. H. Chang, Derivation of the SLEDAI. A disease activity index for lupus patients. The Committee on Prognosis Studies in SLE. *Arthritis and rheumatism* **35**, 630-640 (1992).

64. R. Mallone *et al.*, Isolation and preservation of peripheral blood mononuclear cells for analysis of islet antigen-reactive T cell responses: position statement of the T-Cell Workshop Committee of the Immunology of Diabetes Society. *Clinical and experimental immunology* **163**, 33-49 (2011).

65. K. U. Knowlton, E. S. Jeon, N. Berkley, R. Wessely, S. Huber, A mutation in the puff region of VP2 attenuates the myocarditic phenotype of an infectious cDNA of the Woodruff variant of coxsackievirus B3. *Journal of virology* **70**, 7811-7818 (1996).

66. D. L. Russell, J. M. Dalrymple, R. E. Johnston, Sindbis virus mutations which coordinately affect glycoprotein processing, penetration, and virulence in mice. *Journal of virology* **63**, 1619-1629 (1989).

67. O. W. Schmidt, M. K. Cooney, G. E. Kenny, Plaque assay and improved yield of human coronaviruses in a human rhabdomyosarcoma cell line. *Journal of clinical microbiology* **9**, 722-728 (1979).

68. A. Rohnstock, L. Lehmann, Evaluation of the probe dihydrocalcein acetoxymethylester as an indicator of reactive oxygen species formation and comparison with oxidative DNA base modification determined by modified alkaline elution technique. *Toxicol In Vitro* **21**, 1552-1562 (2007).

69. R. C. Scaduto, Jr., L. W. Grotyohann, Measurement of mitochondrial membrane potential using fluorescent rhodamine derivatives. *Biophysical journal* **76**, 469-477 (1999).

70. M. B. de Moura, B. Van Houten, Bioenergetic analysis of intact mammalian cells using the Seahorse XF24 Extracellular Flux analyzer and a luciferase ATP assay. *Methods in molecular biology* **1105**, 589-602 (2014).

71. M. C. Fung, S. F. Sia, K. N. Leung, N. K. Mak, Detection of differential expression of mouse interferon-alpha subtypes by polymerase chain reaction using specific primers. *Journal of immunological methods* **284**, 177-186 (2004).

72. M. W. Pfaffl, A new mathematical model for relative quantification in real-time RT-PCR. *Nucleic acids research* **29**, e45 (2001).

73. S. Alberti, R. Halfmann, O. King, A. Kapila, S. Lindquist, A systematic survey identifies prions and illuminates sequence features of prionogenic proteins. *Cell* **137**, 146-158 (2009).

74. S. Schmitt *et al.*, A semi-automated method for isolating functionally intact mitochondria from cultured cells and tissue biopsies. *Analytical biochemistry* **443**, 66-74 (2013).

75. A. C. Nulton-Persson, L. I. Szweda, Modulation of mitochondrial function by hydrogen peroxide. *The Journal of biological chemistry* **276**, 23357-23361 (2001).

76. L. A. Callahan, D. A. Stofan, L. I. Szweda, D. E. Nethery, G. S. Supinski, Free radicals alter maximal diaphragmatic mitochondrial oxygen consumption in endotoxin-induced sepsis. *Free radical biology & medicine* **30**, 129-138 (2001).

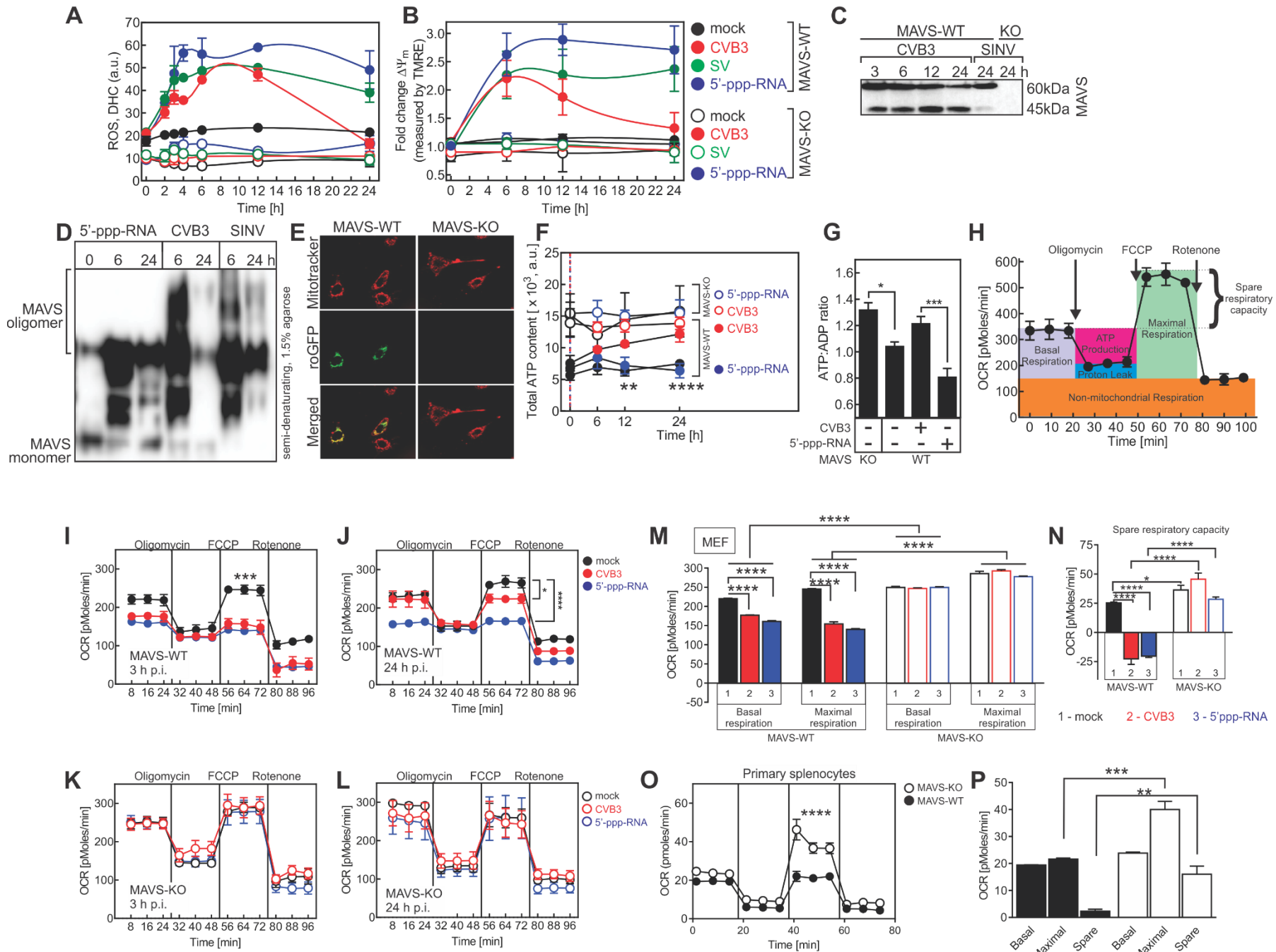
A
ROS, DHC (a.u.)
Time [h]
B
Fold change ΔΨm (measured by TMRE)
mock
CVB3
SV
5'-ppp-RNA
MAVS-WT
MAVS-KO
C
MAVS-WT
KO
CVB3
SINV
3 6 12 24 24 24 h
60kDa
45kDa
MAVS
D
5'-ppp-RNA
CVB3
SINV
0 6 24 6 24 6 24 h
MAVS oligomer
MAVS monomer
semi-denaturating, 1.5% agarose
E
MAVS-WT
MAVS-KO
Mitotracker
roGFP
Merged
F
Total ATP content [x 10^3, a.u.]
Time [h]
G
ATP:ADP ratio
CVB3
5'-ppp-RNA
MAVS KO WT
H
Oligomycin
FCCP
Rotenone
OCR [pMoles/min]
Basal Respiration
ATP Production
Proton Leak
Maximal Respiration
Spare respiratory capacity
Non-mitochondrial Respiration
Time [min]
I
MAVS-WT
3 h p.i.
J
MAVS-WT
24 h p.i.
M
MEF
Basal respiration
Maximal respiration
MAVS-WT
MAVS-KO
N
Spare respiratory capacity
1 - mock
2 - CVB3
3 - 5'ppp-RNA
K
MAVS-KO
3 h p.i.
L
MAVS-KO
24 h p.i.
O
Primary splenocytes
OCR (pmoles/min)
P
Basal
Maximal
Spare

Figure 1

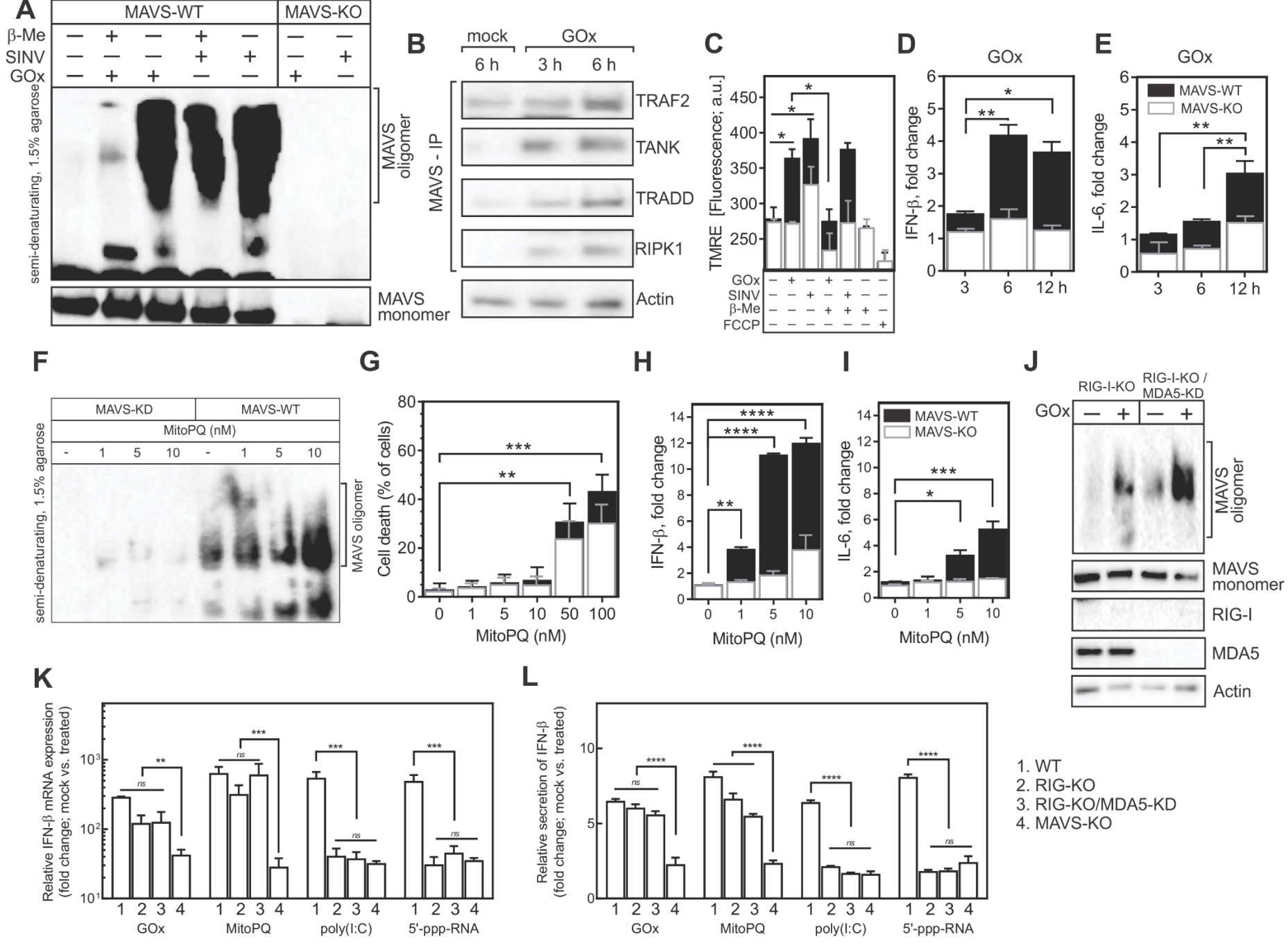
A
MAVS-WT
MAVS-KO
β-Me
SINV
GOx
semi-denaturating, 1.5% agarose
MAVS oligomer
MAVS monomer
B
mock
GOx
6 h
3 h
6 h
MAVS - IP
TRAF2
TANK
TRADD
RIPK1
Actin
C
TMRE [Fluorescence; a.u.]
GOx
SINV
β-Me
FCCP
D
GOx
IFN-β, fold change
3
6
12 h
E
GOx
MAVS-WT
MAVS-KO
IL-6, fold change
3
6
12 h
F
MAVS-KD
MAVS-WT
MitoPQ (nM)
semi-denaturating, 1.5% agarose
MAVS oligomer
G
Cell death (% of cells)
MitoPQ (nM)
H
IFN-β, fold change
MitoPQ (nM)
I
MAVS-WT
MAVS-KO
IL-6, fold change
MitoPQ (nM)
J
RIG-I-KO
RIG-I-KO / MDA5-KD
GOx
MAVS oligomer
MAVS monomer
RIG-I
MDA5
Actin
K
Relative IFN-β mRNA expression (fold change; mock vs. treated)
GOx
MitoPQ
poly(I:C)
5'-ppp-RNA
L
Relative secretion of IFN-β (fold change; mock vs. treated)
GOx
MitoPQ
poly(I:C)
5'-ppp-RNA
1. WT
2. RIG-KO
3. RIG-KO/MDA5-KD
4. MAVS-KO

Figure 2

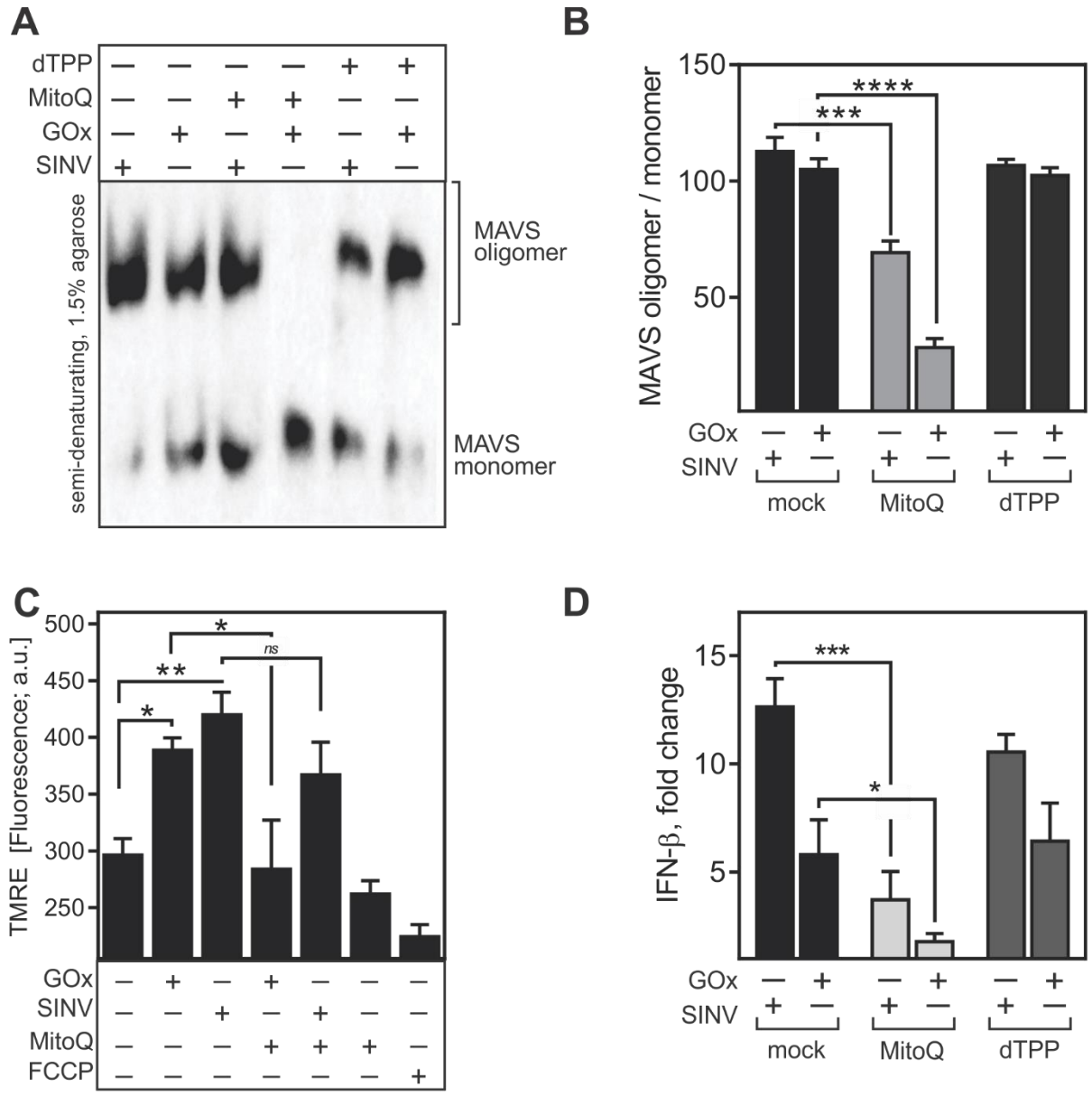
A
dTPP
MitoQ
GOx
SINV
semi-denaturating, 1.5% agarose
MAVS oligomer
MAVS monomer
B
MAVS oligomer / monomer
150
100
50
****
***
GOx
SINV
mock
MitoQ
dTPP
C
TMRE [Fluorescence; a.u.]
500
450
400
350
300
250
*
**
*
ns
GOx
SINV
MitoQ
FCCP
D
IFN-β, fold change
15
10
5
***
*
GOx
SINV
mock
MitoQ
dTPP

Figure 3

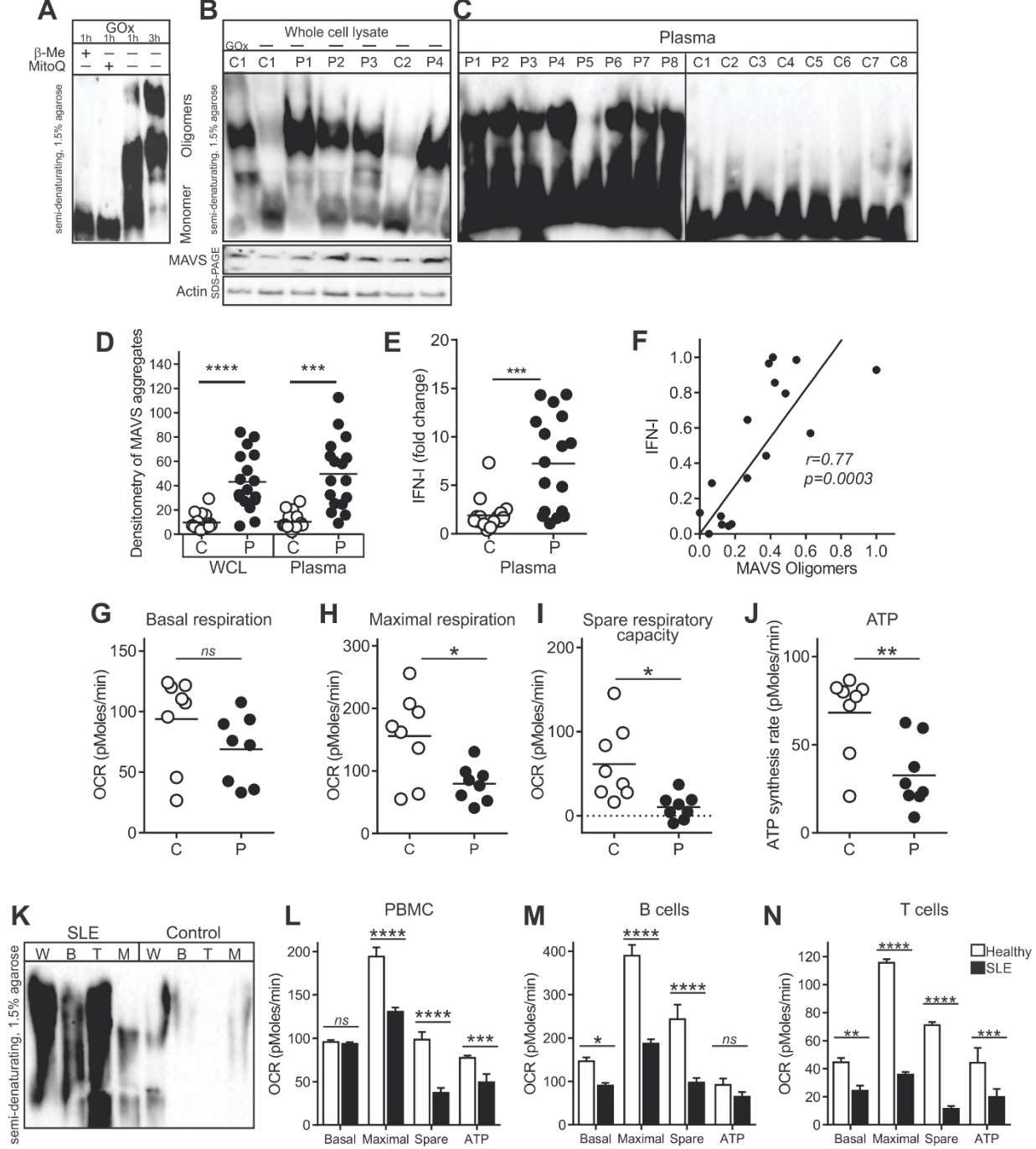
A
GOx
1h 1h 1h 3h
β-Me
MitoQ
semi-denaturating, 1.5% agarose
B
Whole cell lysate
GOx
C1 C1 P1 P2 P3 C2 P4
Oligomers
Monomer
semi-denaturating, 1.5% agarose
MAVS
Actin
SDS-PAGE
C
Plasma
P1 P2 P3 P4 P5 P6 P7 P8 C1 C2 C3 C4 C5 C6 C7 C8
D
Densitometry of MAVS aggregates
****
***
C P C P
WCL Plasma
E
IFN-I (fold change)
***
C P
Plasma
F
IFN-I
r=0.77
p=0.0003
MAVS Oligomers
G
Basal respiration
ns
OCR (pMoles/min)
C P
H
Maximal respiration
*
OCR (pMoles/min)
C P
I
Spare respiratory capacity
*
OCR (pMoles/min)
C P
J
ATP
**
ATP synthesis rate (pMoles/min)
C P
K
SLE
Control
W B T M W B T M
semi-denaturating, 1.5% agarose
L
PBMC
OCR (pMoles/min)
ns
****
****
***
Basal Maximal Spare ATP
M
B cells
OCR (pMoles/min)
*
****
****
ns
Basal Maximal Spare ATP
N
T cells
Healthy
SLE
OCR (pMoles/min)
**
****
****
***
Basal Maximal Spare ATP

Figure 4

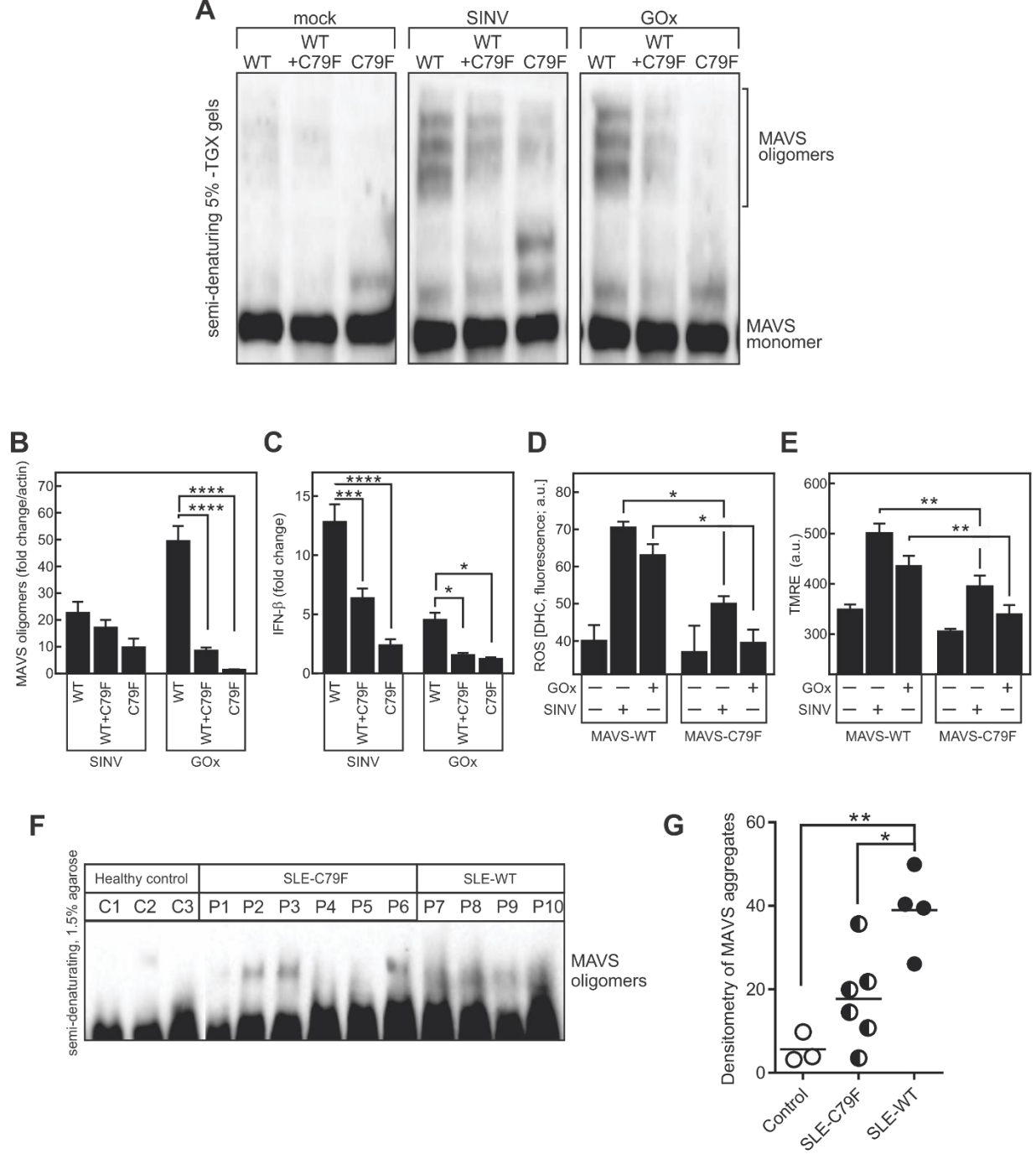
A
mock
SINV
GOx
WT
+C79F
C79F
semi-denaturing 5% -TGX gels
MAVS oligomers
MAVS monomer
B
MAVS oligomers (fold change/actin)
C
IFN-β (fold change)
D
ROS [DHC, fluorescence; a.u.]
E
TMRE (a.u.)
SINV
GOx
MAVS-WT
MAVS-C79F
F
Healthy control
SLE-C79F
SLE-WT
C1 C2 C3 P1 P2 P3 P4 P5 P6 P7 P8 P9 P10
semi-denaturating, 1.5% agarose
MAVS oligomers
G
Densitometry of MAVS aggregates
Control
SLE-C79F
SLE-WT

Figure 5

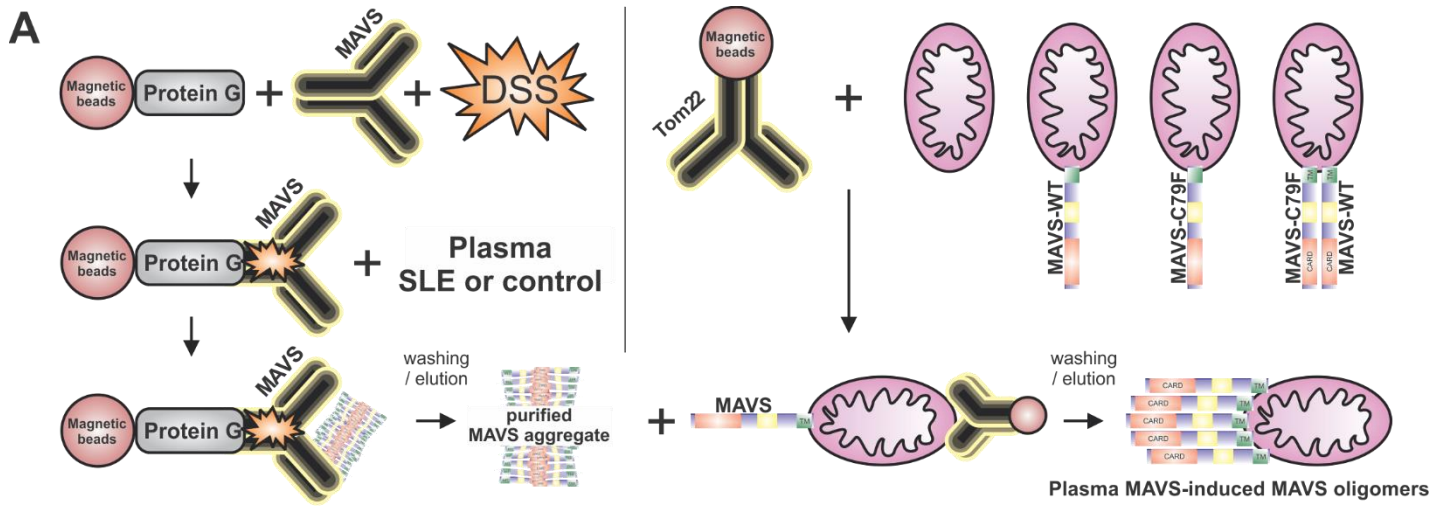
A
Magnetic beads
Protein G
MAVS
DSS
Plasma
SLE or control
washing
/ elution
purified
MAVS aggregate
Tom22
MAVS-WT
MAVS-C79F
MAVS-C79F
MAVS-WT
MAVS
washing
/ elution
Plasma MAVS-induced MAVS oligomers

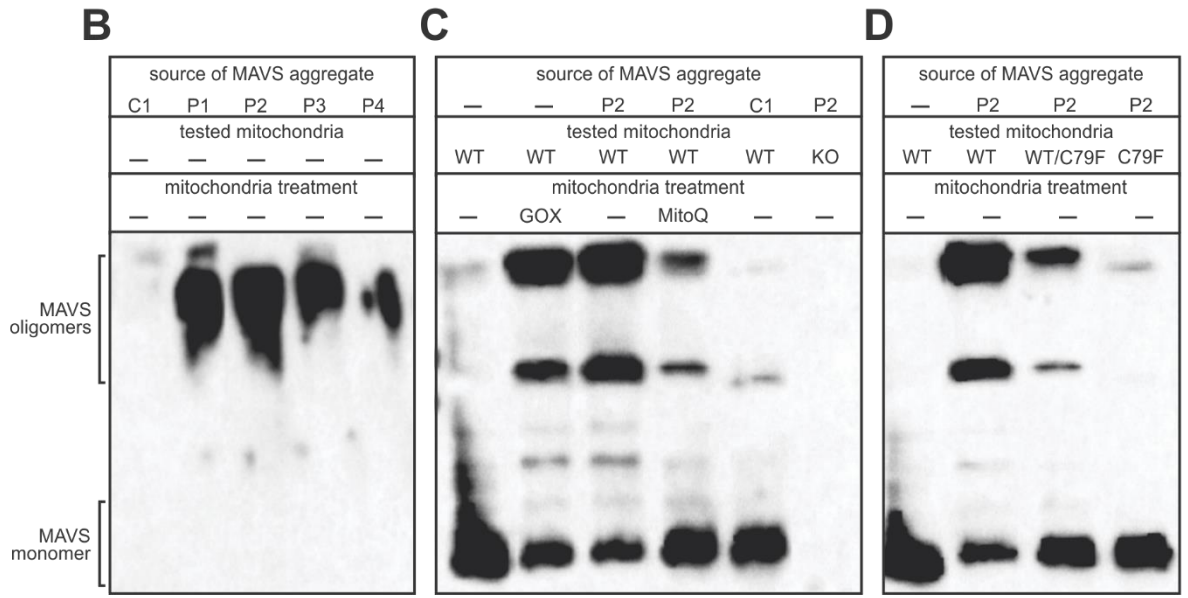
B
source of MAVS aggregate
C1 P1 P2 P3 P4
tested mitochondria
— — — — —
mitochondria treatment
— — — — —
C
source of MAVS aggregate
— — P2 P2 C1 P2
tested mitochondria
WT WT WT WT WT KO
mitochondria treatment
— GOX — MitoQ — —
D
source of MAVS aggregate
— P2 P2 P2
tested mitochondria
WT WT WT/C79F C79F
mitochondria treatment
— — — —
MAVS oligomers
MAVS monomer

Figure 6

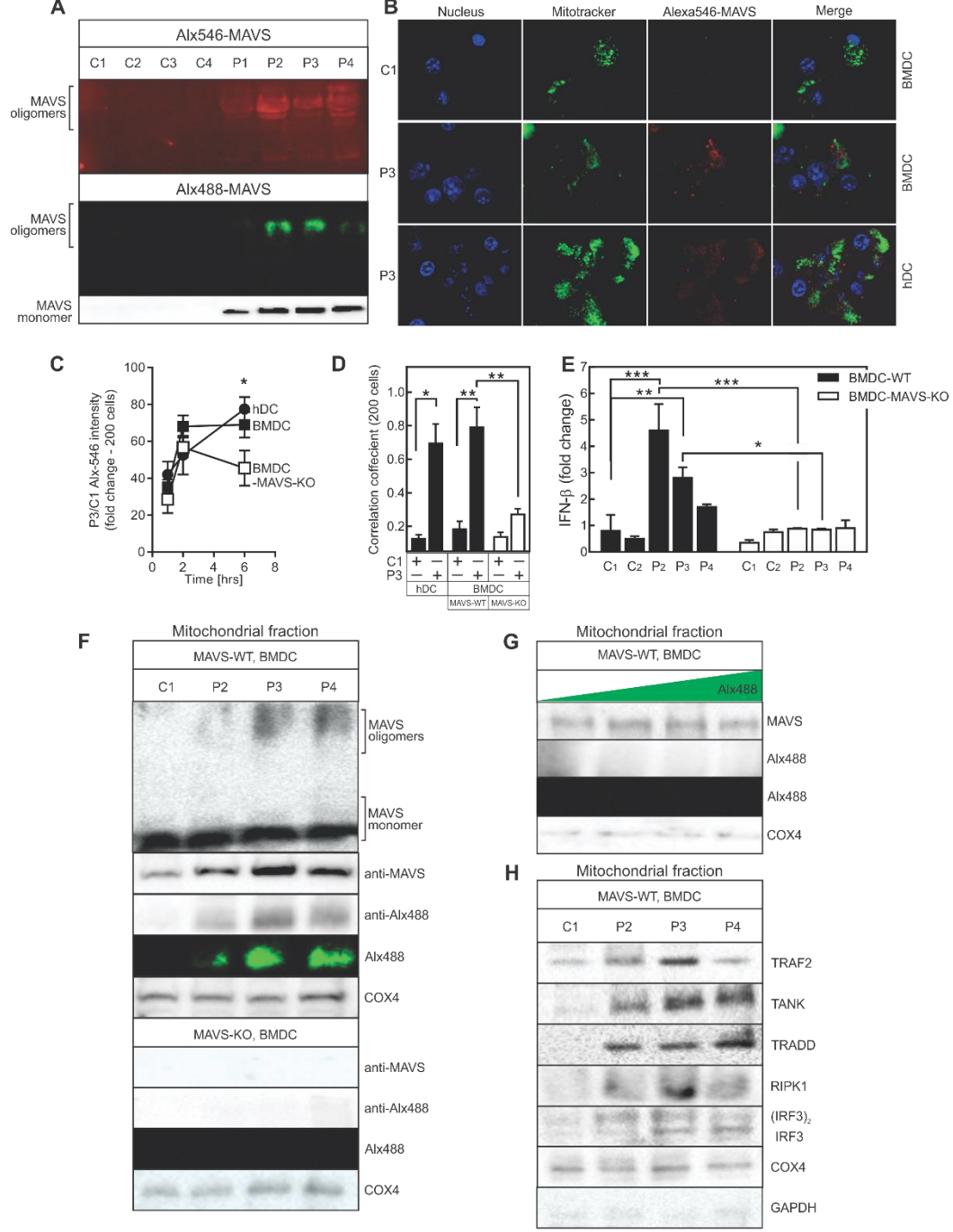
A
Alx546-MAVS
C1 C2 C3 C4 P1 P2 P3 P4
MAVS oligomers
Alx488-MAVS
MAVS oligomers
MAVS monomer
B
Nucleus
Mitotracker
Alexa546-MAVS
Merge
C1
P3
P3
BMDC
BMDC
hDC
C
P3/C1 Alx-546 intensity (fold change - 200 cells)
Time [hrs]
hDC
BMDC
BMDC -MAVS-KO
D
Correlation coffecient (200 cells)
C1
P3
hDC
BMDC
MAVS-WT
MAVS-KO
E
IFN-β (fold change)
BMDC-WT
BMDC-MAVS-KO
C1 C2 P2 P3 P4 C1 C2 P2 P3 P4
F
Mitochondrial fraction
MAVS-WT, BMDC
C1 P2 P3 P4
MAVS oligomers
MAVS monomer
anti-MAVS
anti-Alx488
Alx488
COX4
MAVS-KO, BMDC
anti-MAVS
anti-Alx488
Alx488
COX4
G
Mitochondrial fraction
MAVS-WT, BMDC
Alx488
MAVS
Alx488
Alx488
COX4
H
Mitochondrial fraction
MAVS-WT, BMDC
C1 P2 P3 P4
TRAF2
TANK
TRADD
RIPK1
(IRF3)2
IRF3
COX4
GAPDH

Figure 7

SUPPLEMENTARY MATERIALS

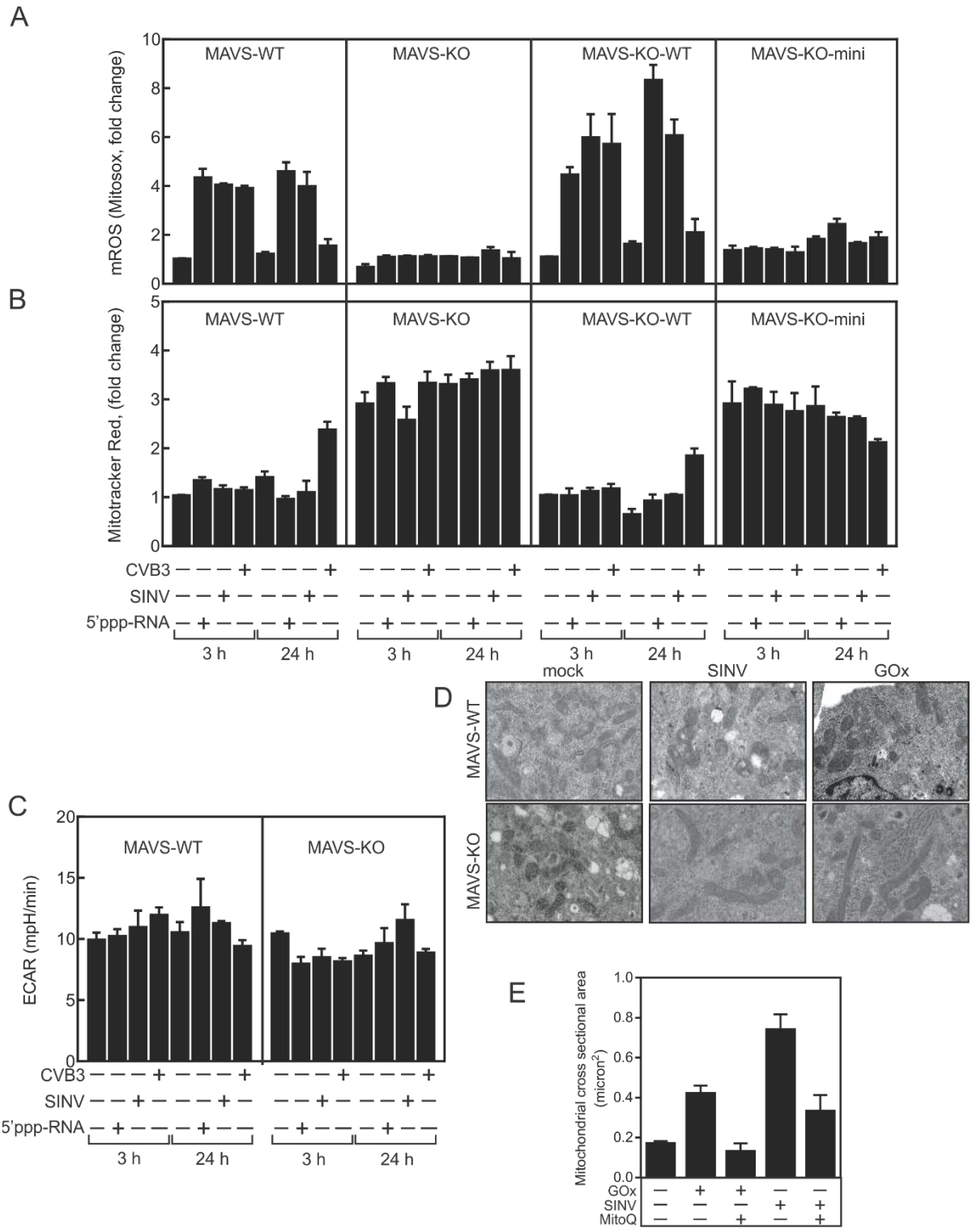

Supplementary Figure 1. Measurement of mROS, mitochondrial mass and mitochondrial phenotype. (A) Generation of mROS in WT, MAVS-deficient, reconstituted, or minimal-MAVS (truncated at position Gln148) expressing MEF in response to infection with CVB3 or SINV, or transfection with 5′-ppp–RNA, was quantified by FACS using 50 nM MitoSox Red. (B) Flow cytometric quantification of total mitochondrial mass in these cells was achieved by MitoTracker DeepRed. (C) The basal extracellular acidification rate (ECAR), a readout of lactate production by glycolysis, was measured by Seahorse Flux Analyzer. (D) The ultrastructural morphology of mitochondria in WT and MAVS-deficient MEFs following infection was observed by transmission electron microscopy. (E) The dimensions of WT and MAVS-deficient mitochondria were calculated from representative electron microscopic images, and the percentage of elongated mitochondria was calculated from 5 micrographs.

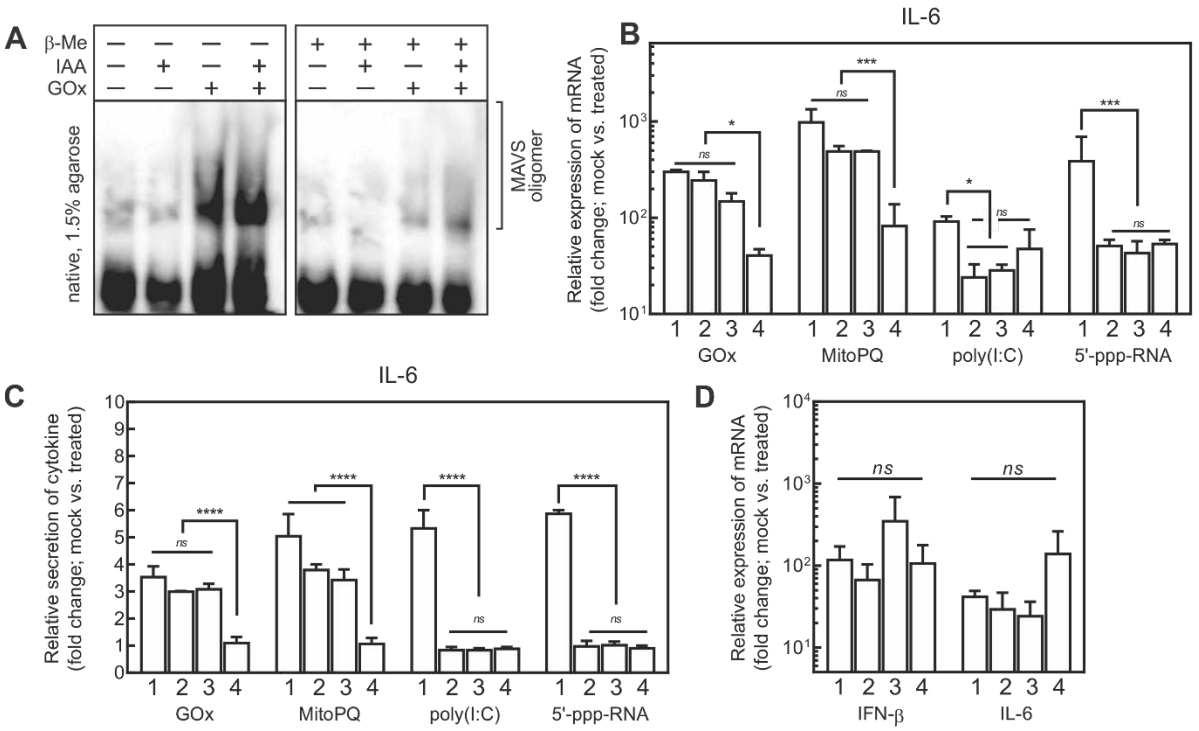

Supplementary Figure 2. MAVS oligomers are not artificially formed during sample processing, homogenization or lysis, and IL-6 expression and secretion in the presence of ROS is independent of RIG-I helicases. (A) Freshly prepared PBMC were treated with GOx or infected with SINV, and subsequently homogenized in buffer containing 100 µM iodoacetamide. (B) Transcriptional activity and secretion of IL-6 in WT (1), RIG-I-KO (2), RIG-I-KO/MDA5-KD (3) and MAVS-KO (4) MEFs in response to GOx, MitoPQ, poly(I:C) and 5'-ppp-RNA was measured by (B) qPCR and (C) ELISA. One-way ANOVA was used for statistical analysis of IFN-² and IL-6 mRNA expression and secretion (*p < 0.05, ***p < 0.005, ****p < 0.0005). (D) As a control, dsDNA treatment was used to determine by qPCR whether WT, RIG-I-KO, RIG-I-KO/MDA5-KD and MAVS-KO MEFs can upregulate IFN-² and IL-6 mRNA in a RIG-I-like independent manner. Statistical analysis by one-way ANOVA of mRNA expression showed non-statistical (ns) differences.

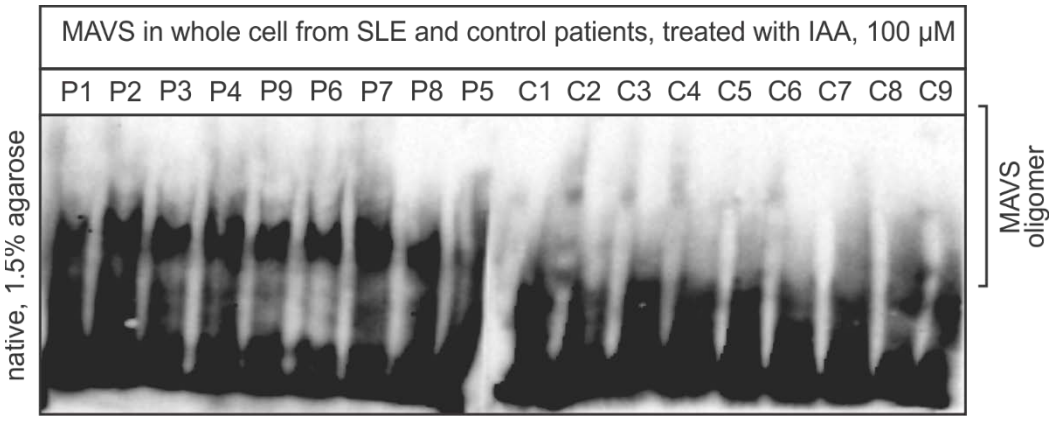

Supplementary Figure 3. MAVS oligomers are not artificially formed during processing, homogenization or lysis of SLE patient samples.

PBMC of SLE patients (n=9) and healthy, sex-and age matched control donors (n=9) were isolated by Ficoll gradient centrifugation as described, and cells and corresponding plasma samples were supplemented with 100 µM iodoacetamide before analysis.

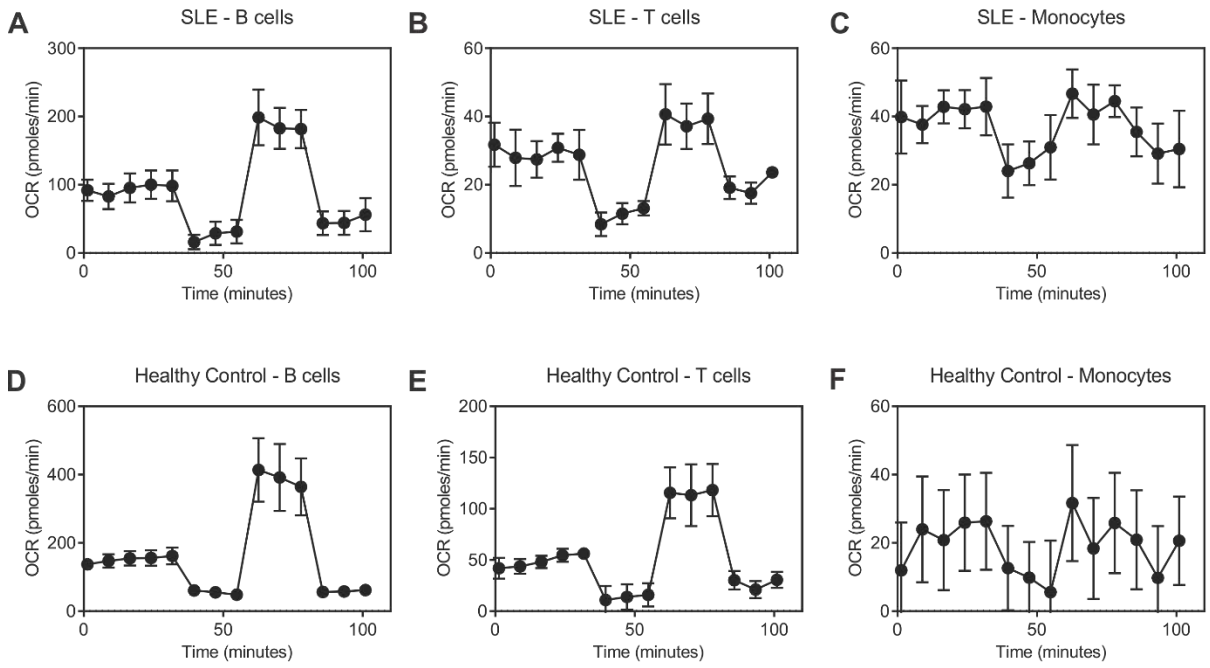

Supplementary Figure 4. Analysis of mitochondrial respiration in PBMC subpopulations. OCR in B cells (A), T cells (B) and monocytes (C) isolated from patients with SLE was measured following the sequential addition of oligomycin, FCCP, and a combination of antimycin A and rotenone. B cells, T cells and monocytes (D, E, and F, respectively) from healthy individuals served as controls. Shown are representative data of three independent experiments.